Energy Storage material status and challenges for KSA and practical application of 3D holey-graphene structure

Imran Shakir

Energy Storage Research Group

Objective

Development of low-cost, high-performance functional materials for large-scale, affordable storage devices for portable electronics, vehicle electrification, smart grid as well as the broad-scale deployment of alternative energy resources such as solar and wind.

Portable electronics

20-30% CO_2 emission

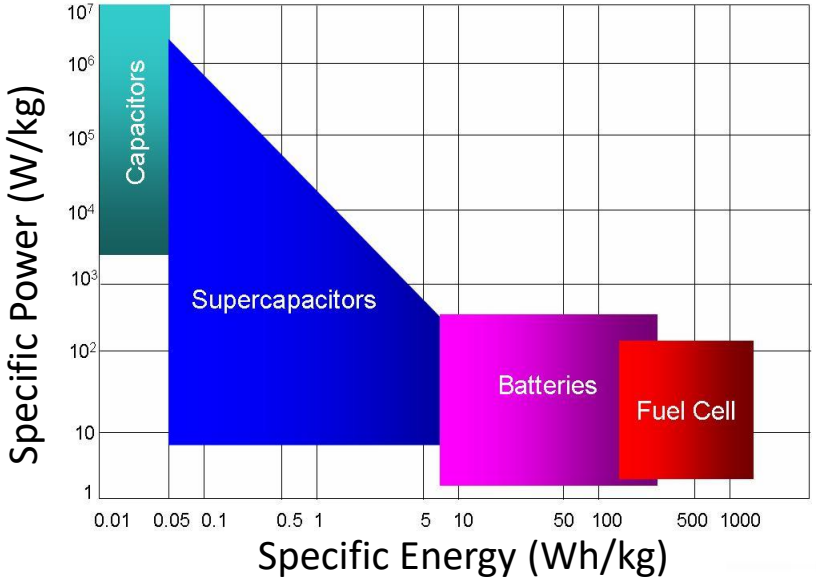

Energy storage is one of the key challenges we face in the 21st century

ELECTROCHEMICAL ENERGY TECHNOLOGIES

Alternative Energy Technologies

- Solar, wind, nuclear, hydro, geothermal, fuel cells, batteries, supercapacitors
- Fuel cells, batteries, supercapacitors: Only viable option for automobiles (~ 30%)
- Batteries: Critical for storing and efficiently utilizing solar and wind energies

Fuel Cell

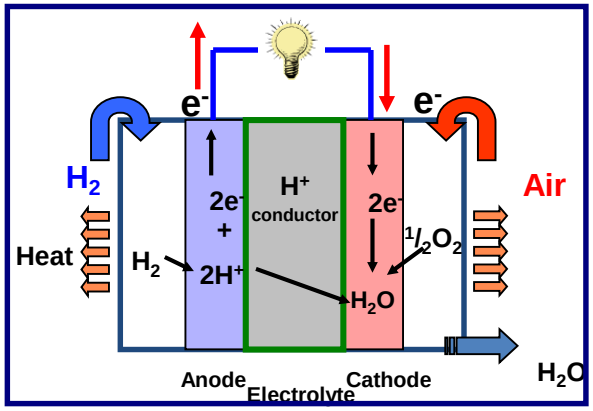

Conversion Device

Portable, transportation, & stationary

Battery

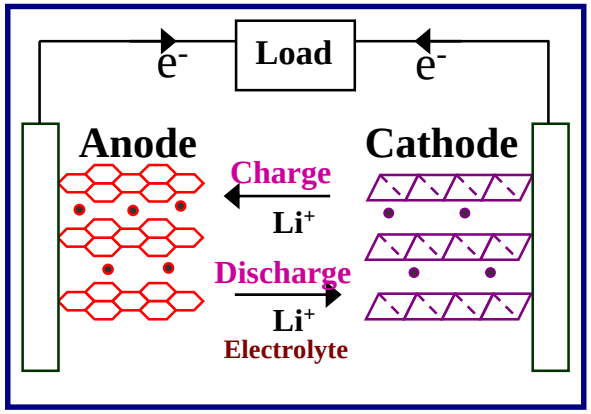

Storage Device

Portable, transportation, & stationary

Supercapacitor

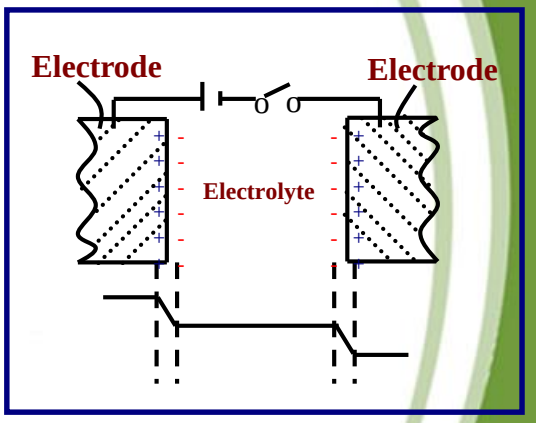

Storage Device

Portable & transportation

- Chemical energy directly into electrical energy – clean energy technologies
- **Challenges:** high cost, safety, durability, & operability problems

Current Energy Storage Devices

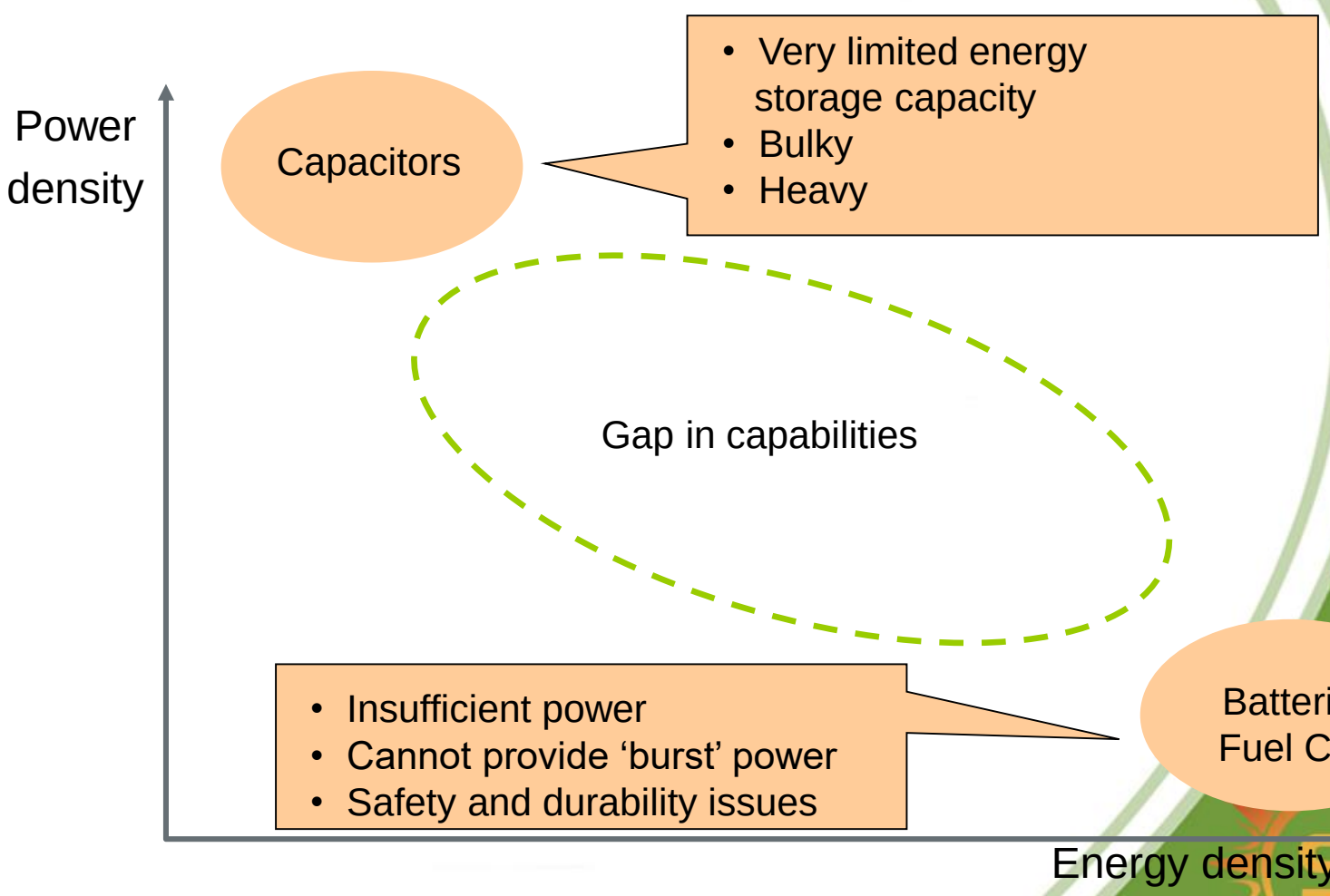

Current Energy Storage Devices

Supercapacitors have a unique ability to provide a solution that is small, lightweight and has the power to fill the gap in capabilities

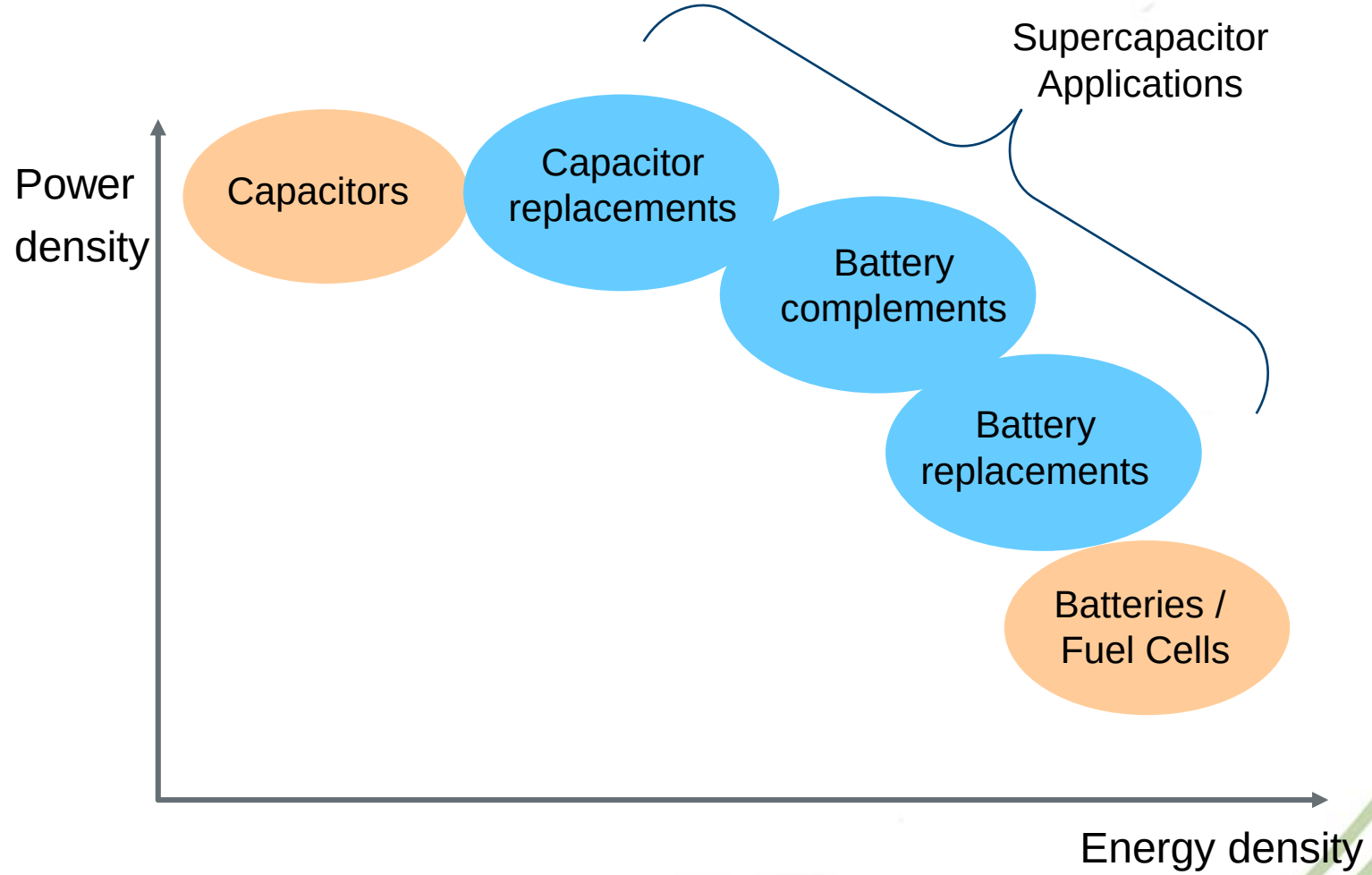

Energy Storage Devices

Capacitor

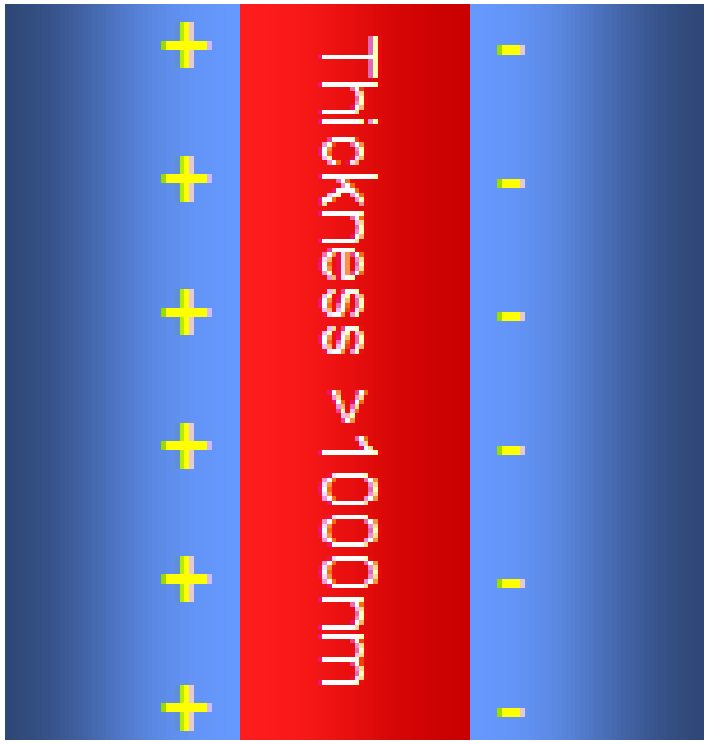

Supercapacitor

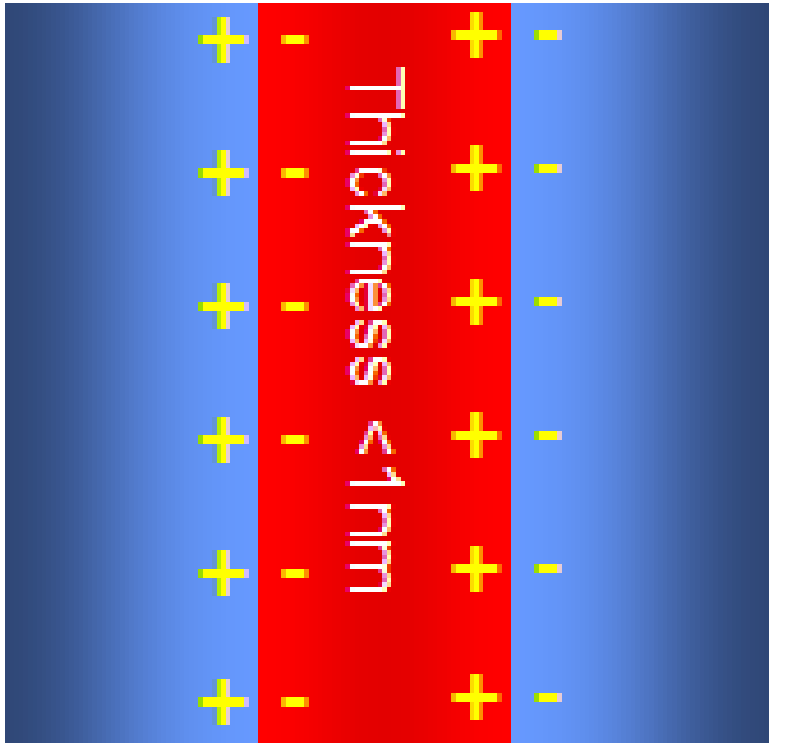

$C \alpha 1/\text{thickness}$

$E = \frac{1}{2} CV^2$

Electrolyte solution

Energy Storage Devices

Batteries

Electrolyte solution

Capacitors and Super-capacitors are surface Storage

Batteries are bulk Storage

Materials Challenges

Reactions occur at the electrode surfaces

- ✓ We want to get as high a surface area as possible
  - Need to have ions and electrons together for reactions to occur
  - However
  - e.g. Nanoparticles behave differently than bulk materials
    - Energy of the reactions also depend on the surface properties
- ✓ Electrons must still be able to get outside the cell
  1. Electron resistance cannot be too high
  2. Separator must be robust and allow rapid transfer of ions
  3. Fundamental materials properties need to be understood

Materials Requirements

- Large reversible capacity
- Small irreversible capacity
- Desirable charge profile
- Desirable kinetics (rate capability)
- Long cycle and calendar life
- Ease of processing
- Safety
- Compatibility with electrolyte and binder systems
- Low cost

Nanotechnology For Energy Storage

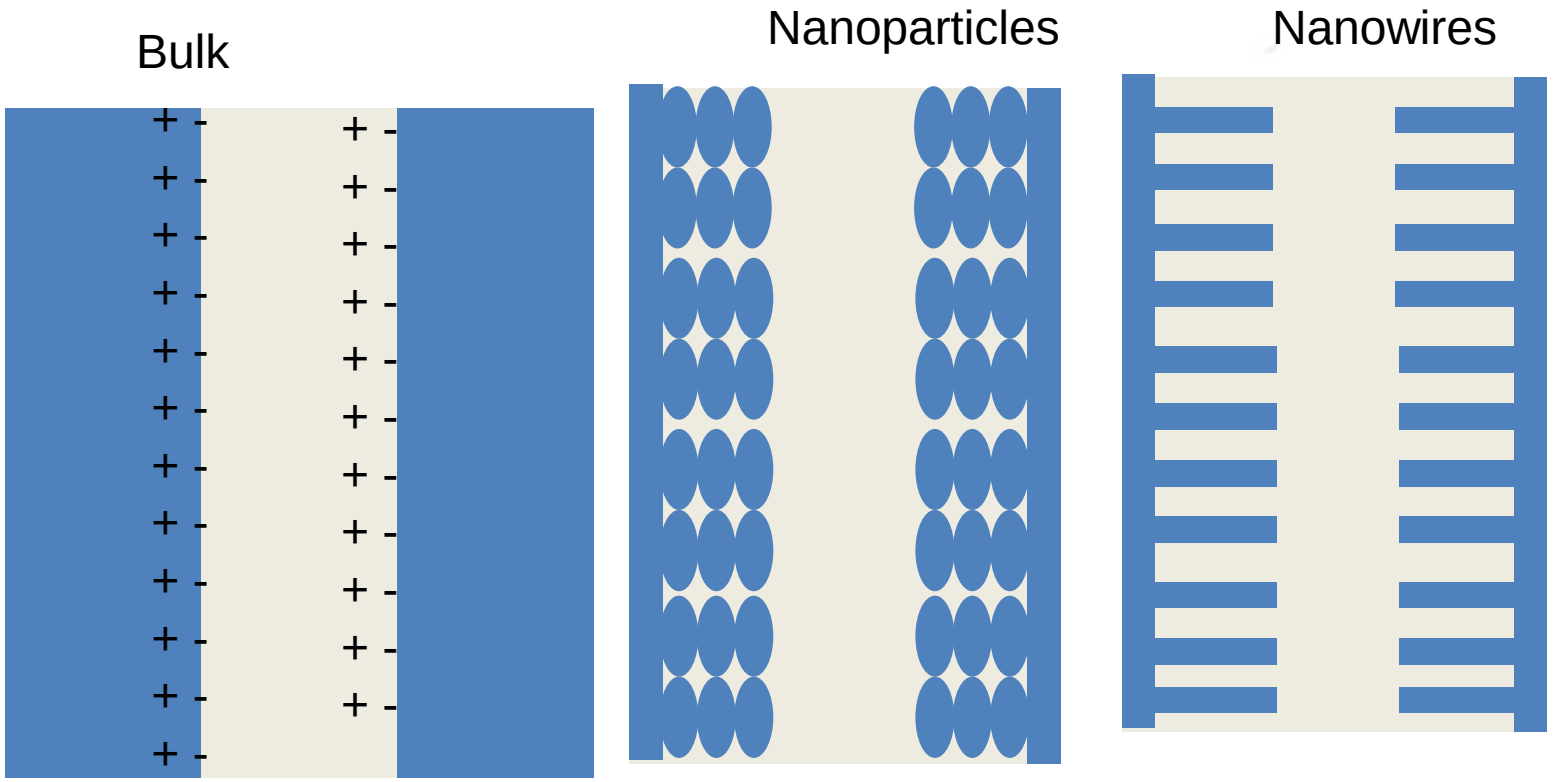

NATURE MATERIALS, VOL 9, FEBRUARY 2010

Chem. Commun., 2010, 46, 4324–4326

Background on graphene

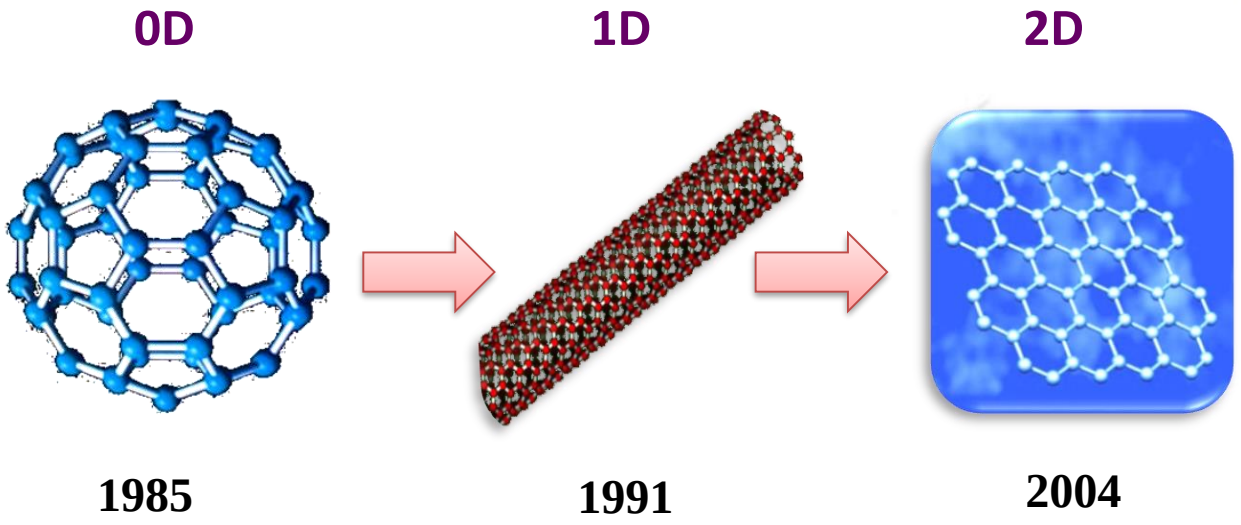

- **Electronic properties** (ballistic transport, high carrier mobility)
- **Mechanical properties** (~1.1 TPa modulus, ~130 Gpa fracture strength)
- **Thermal conductivity** (~5300 W m^{-1} K^{-1} in plane, highly anistropic)
- **Optical transmittance** (97.7%)
- **Specific surface area** (theoretical: 2630 m^2 g^{-1})
- **Specific Capacitance** (theoretical: 550 Fg^{-1})

Potential Applications

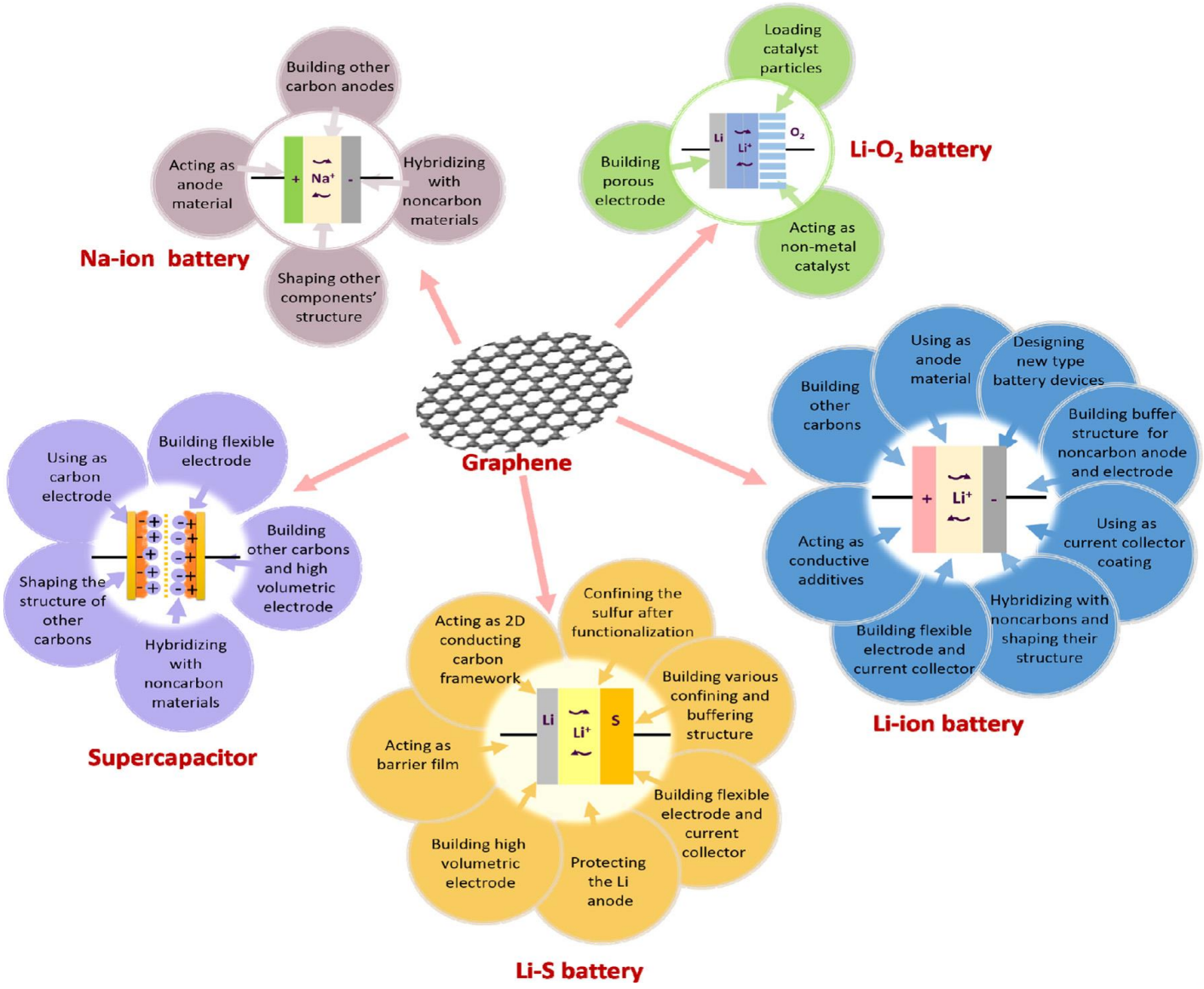

Energy Storage Materials Volume 2, January 2016, Pages 107–138

Preparation of graphene

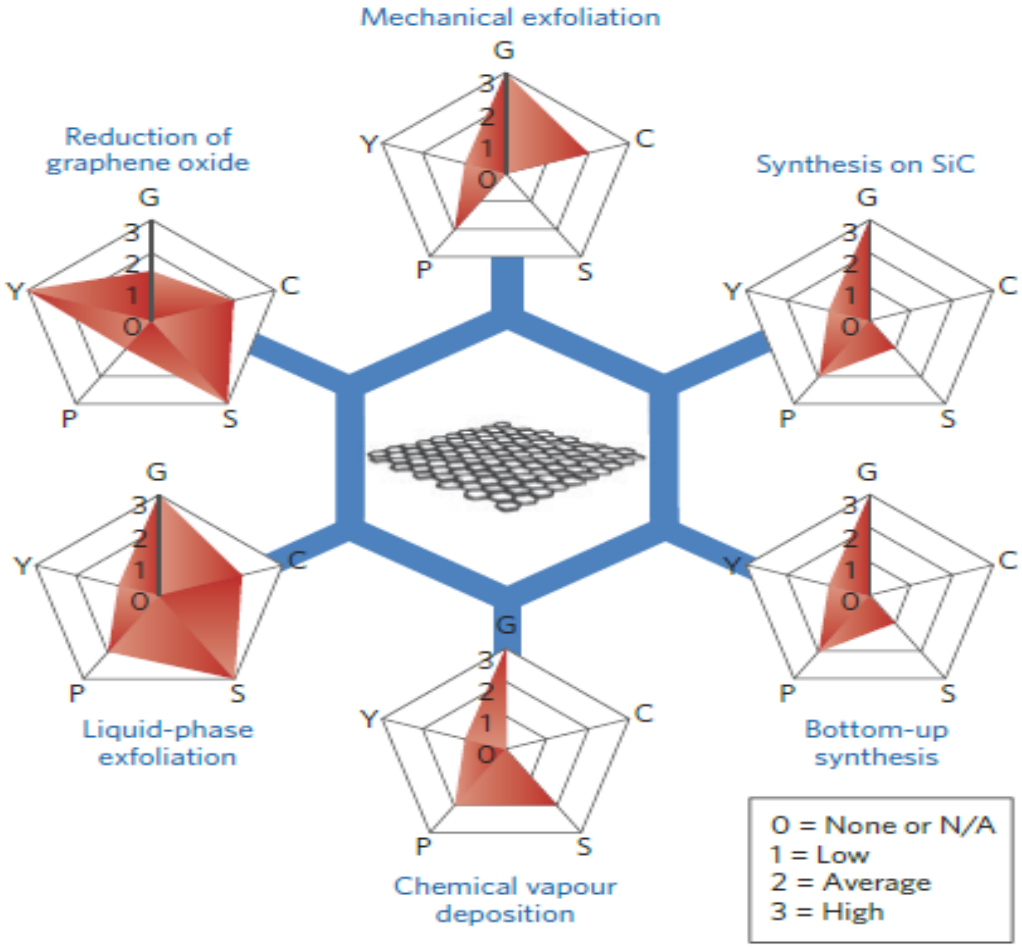

Schematic of the most common graphene production methods. Each method has been evaluated in terms of graphene quality (G), cost aspect (C; a low value corresponds to high cost of production), scalability (S), purity (P) and yield (Y) of the overall production process.

NATURE MATERIALS, VOL 14, 271-279 (2015)

Preparation of Graphene Based Composites

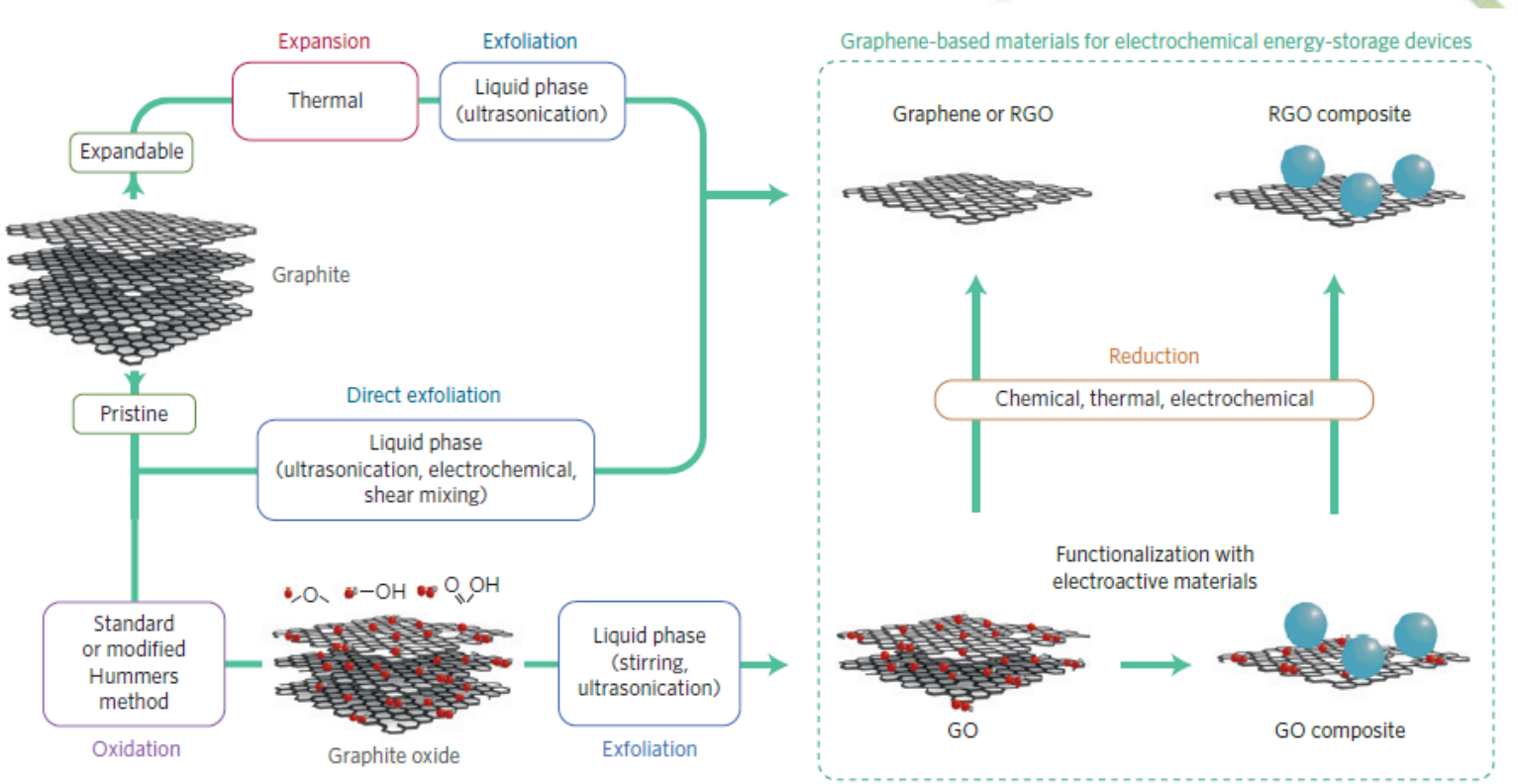

The most common synthetic pathways for producing graphene-based materials (GO, RGO, GO- and RGO-based compounds) for use as electrode active materials in EESDs.

NATURE MATERIALS, VOL 14, 271-279 (2015)

Preparation of Graphene Based Composites

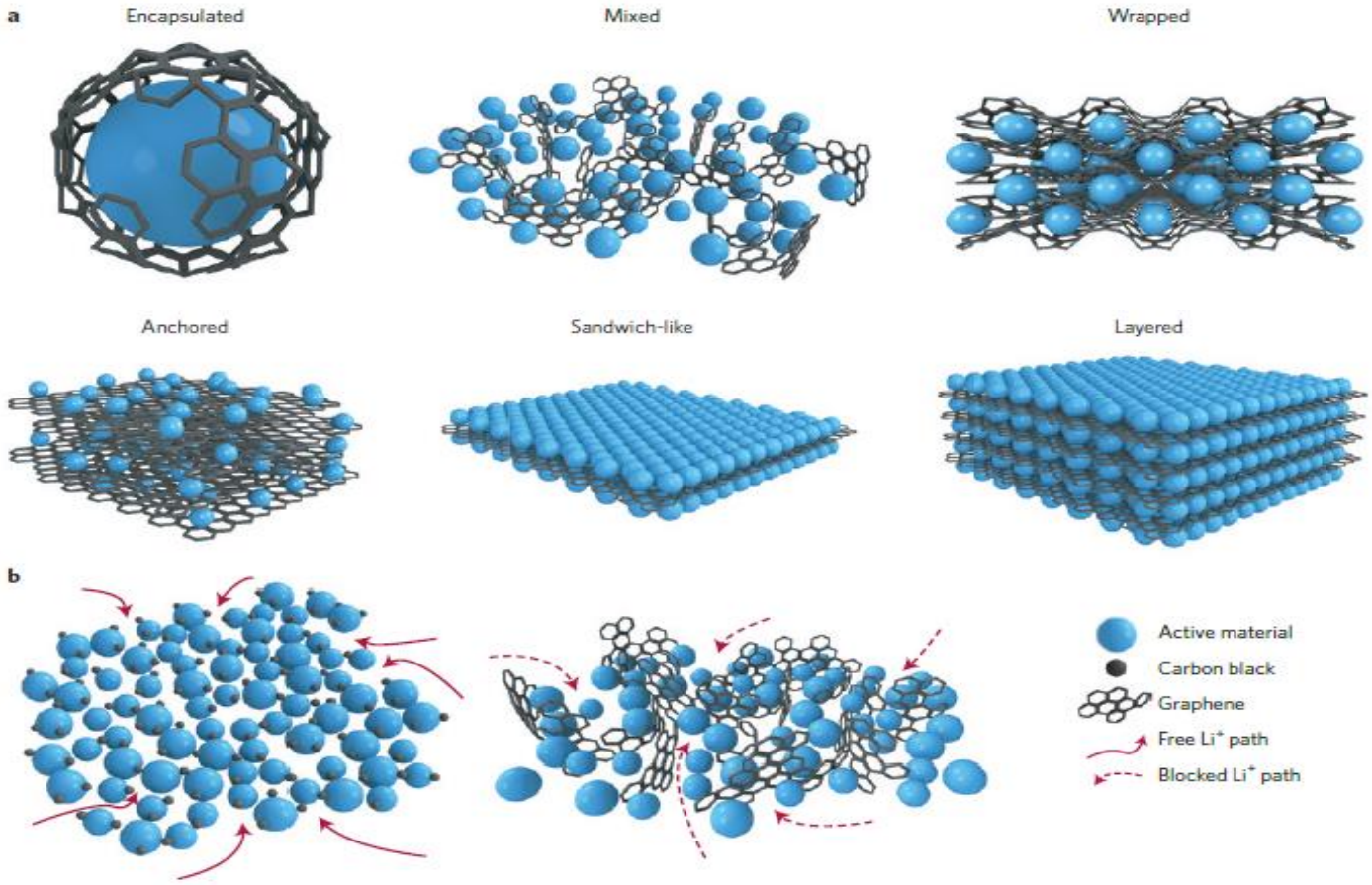

Structural models and a possible drawback of graphene composites.

NATURE MATERIALS, VOL 14, 271-279 (2015)

Potential Applications of 3D Graphene Composites

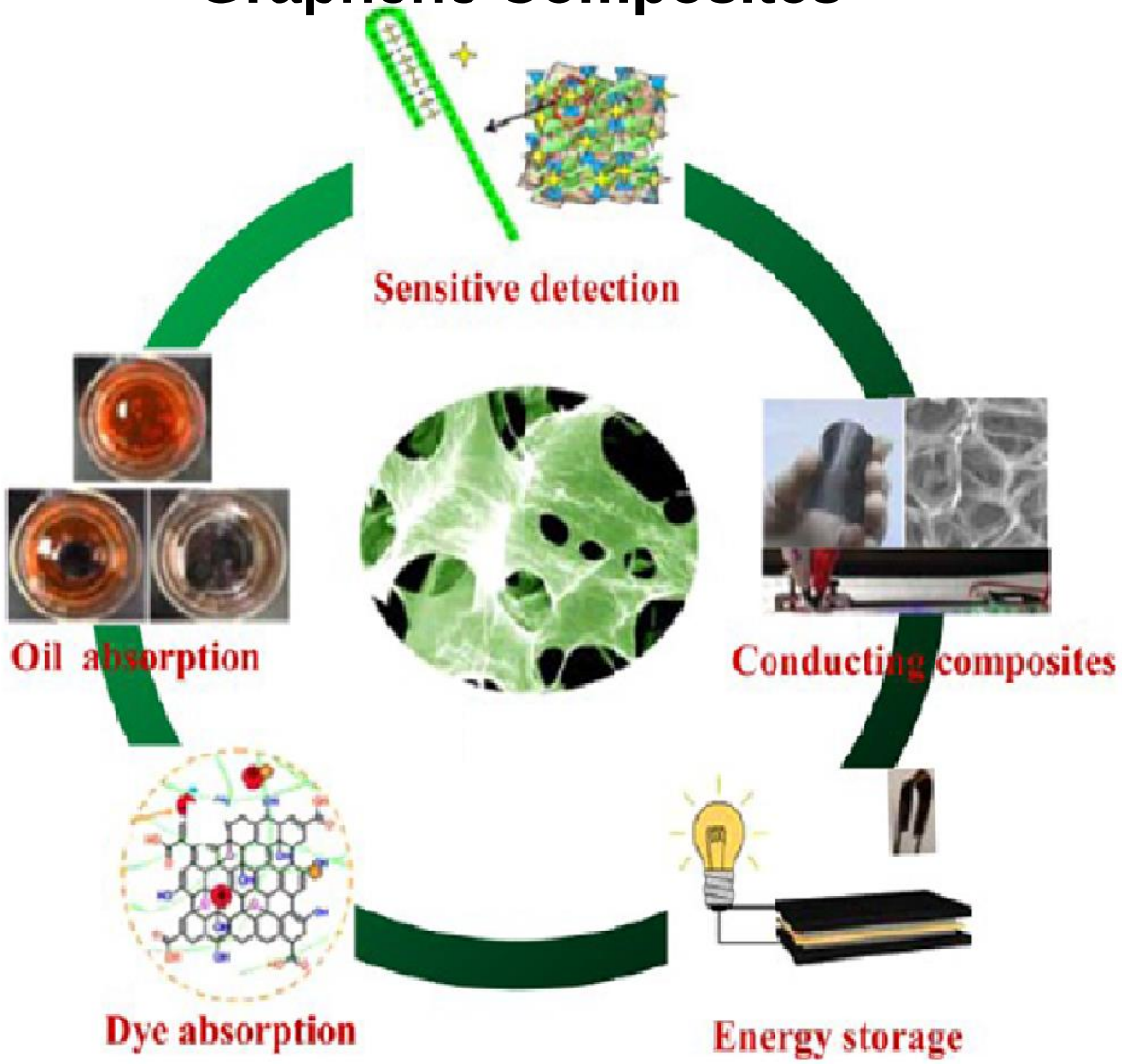

ACS Nano 2016, 10, 7231−7247.

Solution Processable Holey Graphene Oxide and Its Derived Macrostructures for High-Performance Supercapacitors

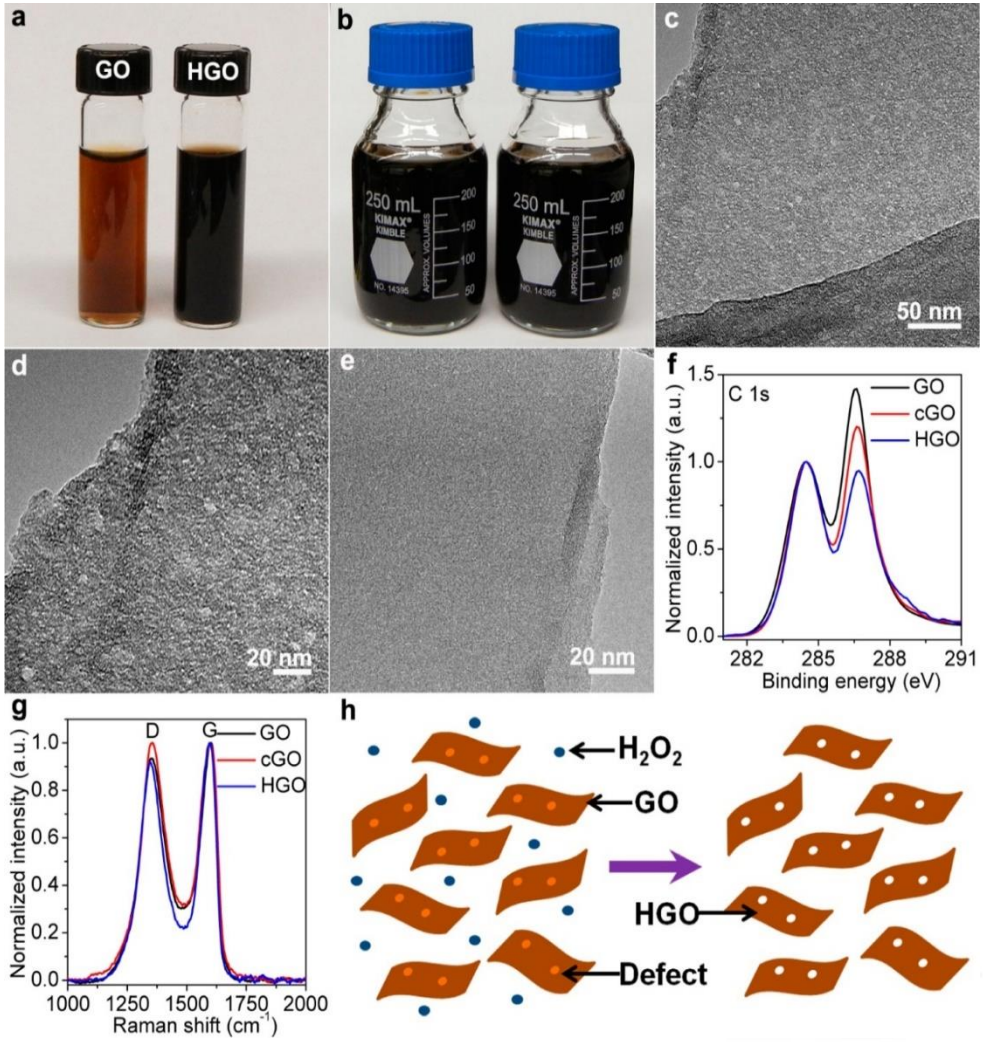

GO was prepared by oxidation of natural graphite powder according to the modified Hummers' method.

HGO was prepared according to the following procedure: Typically, 5 mL 30% H_2O_2 aqueous solution was mixed with 50 mL 2 mg/mL GO aqueous dispersion and then heated at 100 °C for 4 h under stirring.

HGHs were prepared according to the following procedure: 0.5 mL 1 M sodium ascorbate aqueous solution was added into 10 mL 2 mg/mL HGO aqueous dispersion and then the homogeneous mixture was heated at 100 °C for 2 h without stirring

Nano Lett. 2015, 15, 4605.

Solution Processable Holey Graphene Oxide and Its Derived Macrostructures for High-Performance Supercapacitors

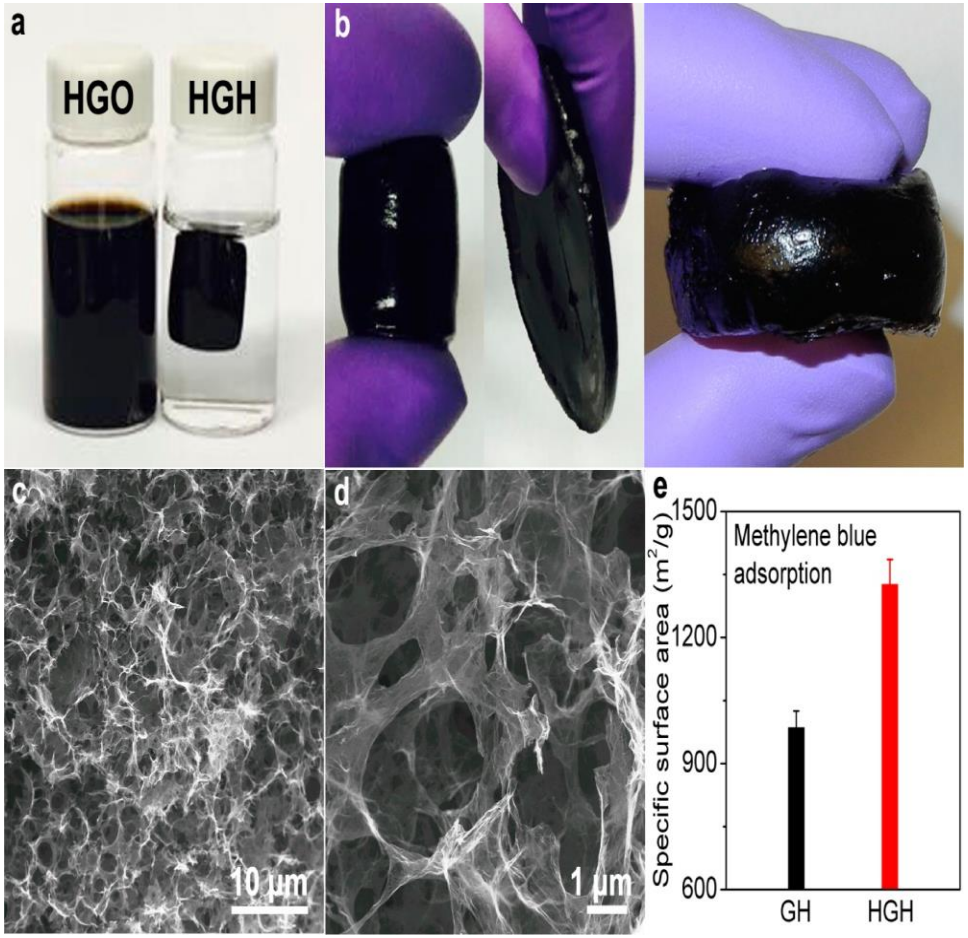

With the flexible processability of HGO dispersion, the sizes and shapes of HGH can be easily tailored by changing the type of reactors. The freeze-dried HGH showed an interconnected 3D porous network with the pore size ranging from submicrometers to several micrometers.

The HGH showed a very high accessible SSA of ~1330 m^2/g, ~34% higher than that of GH (~990 m^2/g),

With the flexible processability of HGO dispersion, the sizes and shapes of HGH can be easily tailored by changing the type of reactors.

Nano Lett. 2015, 15, 4605.

Solution Processable Holey Graphene Oxide and Its Derived Macrostructures for High-Performance Supercapacitors

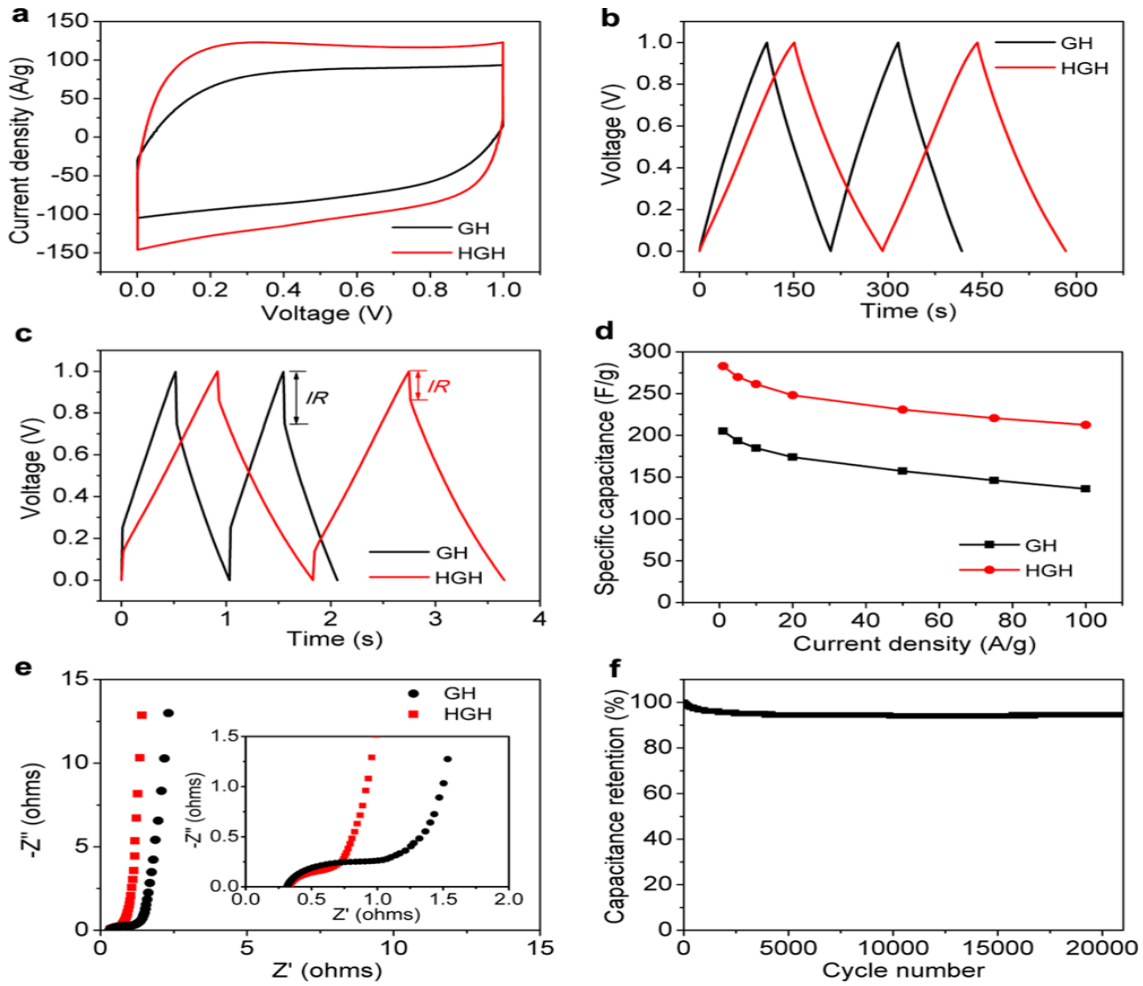

The HGH exhibited a specific capacitance of 283 F/g at a current density of 1 A/g, 38% higher than that of GH (205 F/g)

Nano Lett. 2015, 15, 4605.

Solution Processable Holey Graphene Oxide and Its Derived Macrostructures for High-Performance Supercapacitors

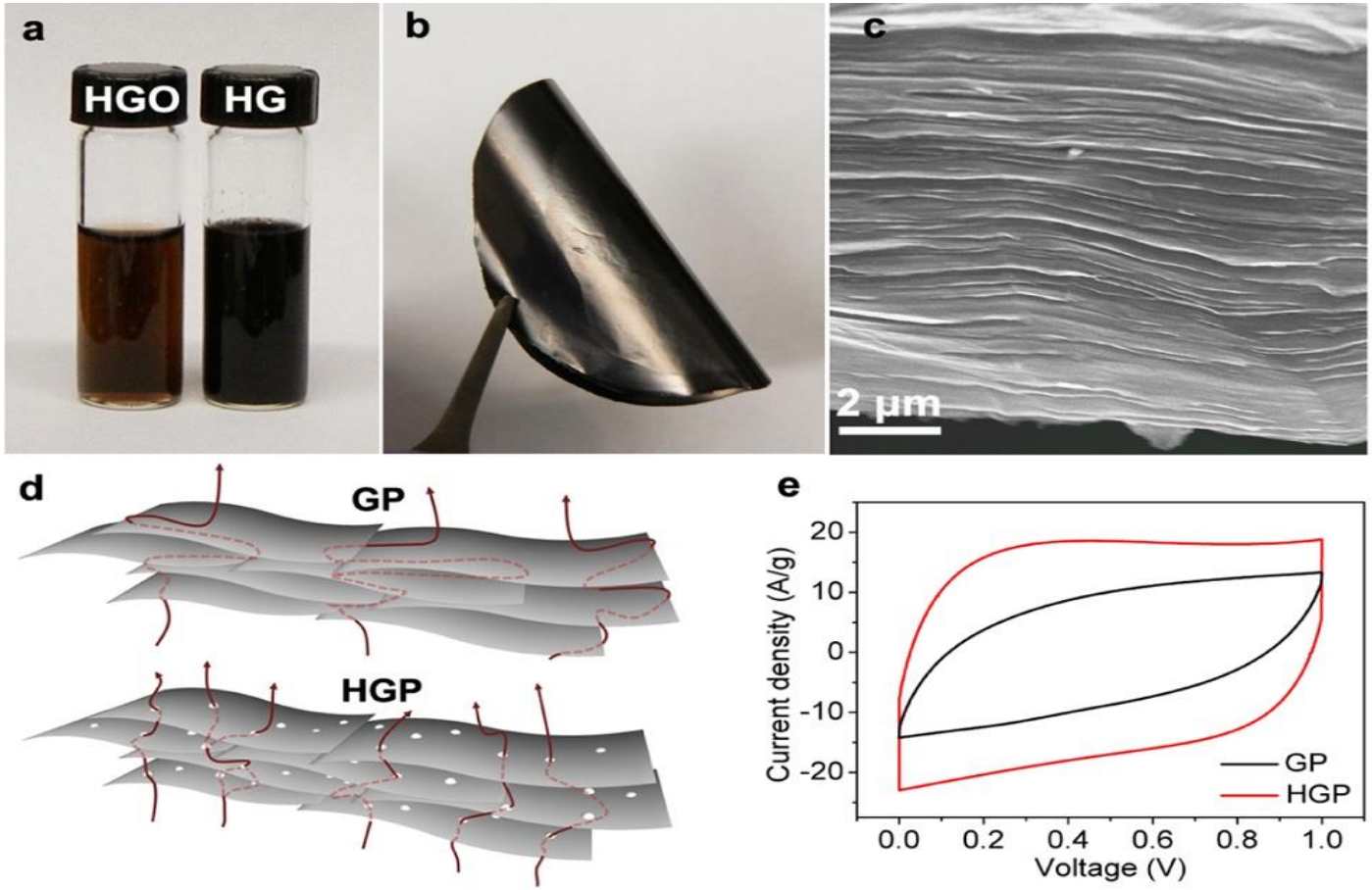

By chemical reduction of the HGO dispersion, we can also obtain well-dispersed solution processable HG which can be further assembled into large-area flexible HGP with a compact layered structure via a flow-directed self assembly strategy .

Nano Lett. 2015, 15, 4605.

Solution Processable Holey Graphene Oxide and Its Derived Macrostructures for High-Performance Supercapacitors

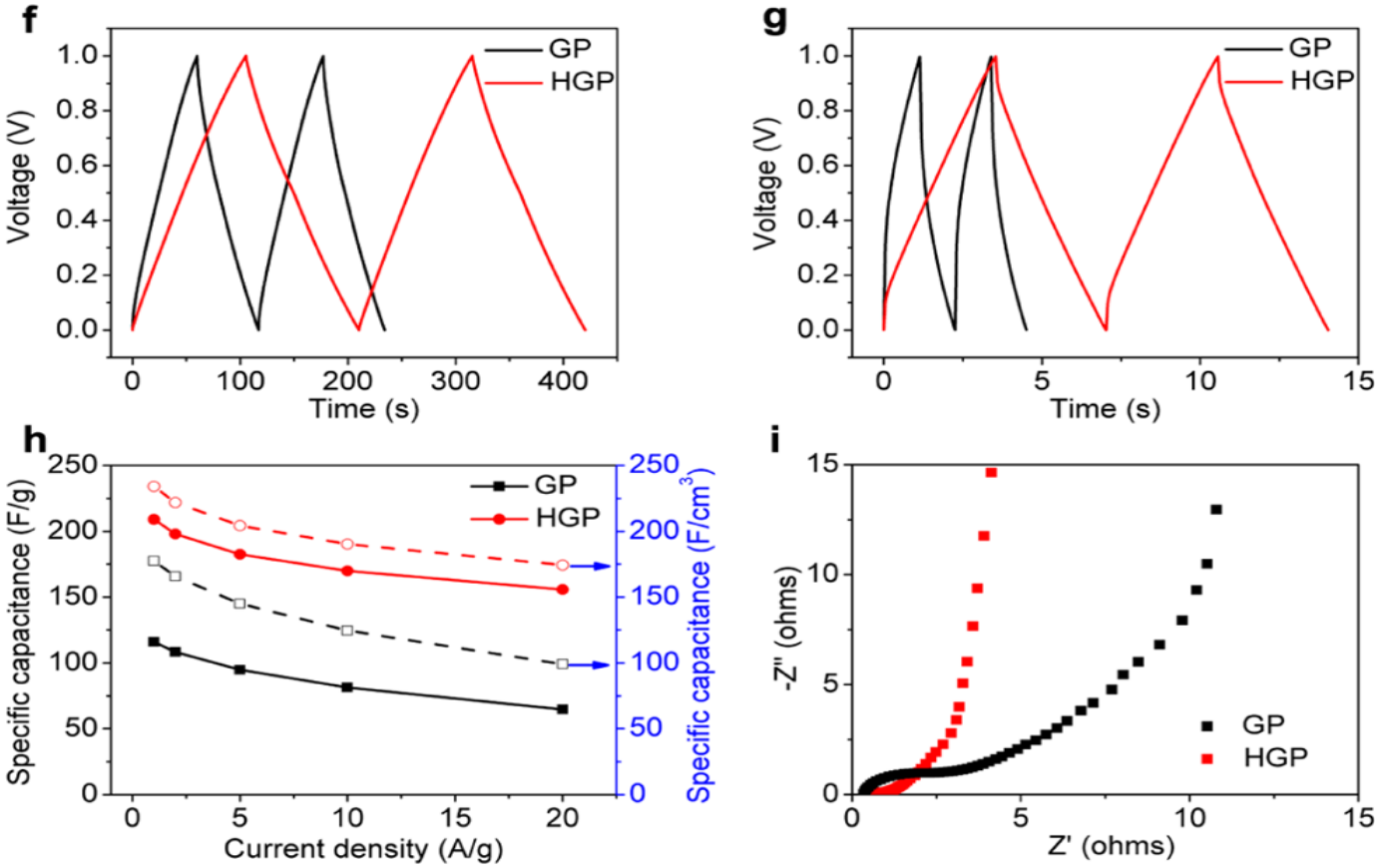

The HGP exhibited a specific capacitance of 209 F/g at 1 A/g, respectively, considerably higher than those of GP (116 F/g). With a high packing density of 1.12 g/cm^3, the HGP could deliver an ultrahigh volumetric capacitance of 234 F/cm^3.

Nano Lett. 2015, 15, 4605.

Solution Processable Holey Graphene Oxide and Its Derived Macrostructures for High-Performance Supercapacitors

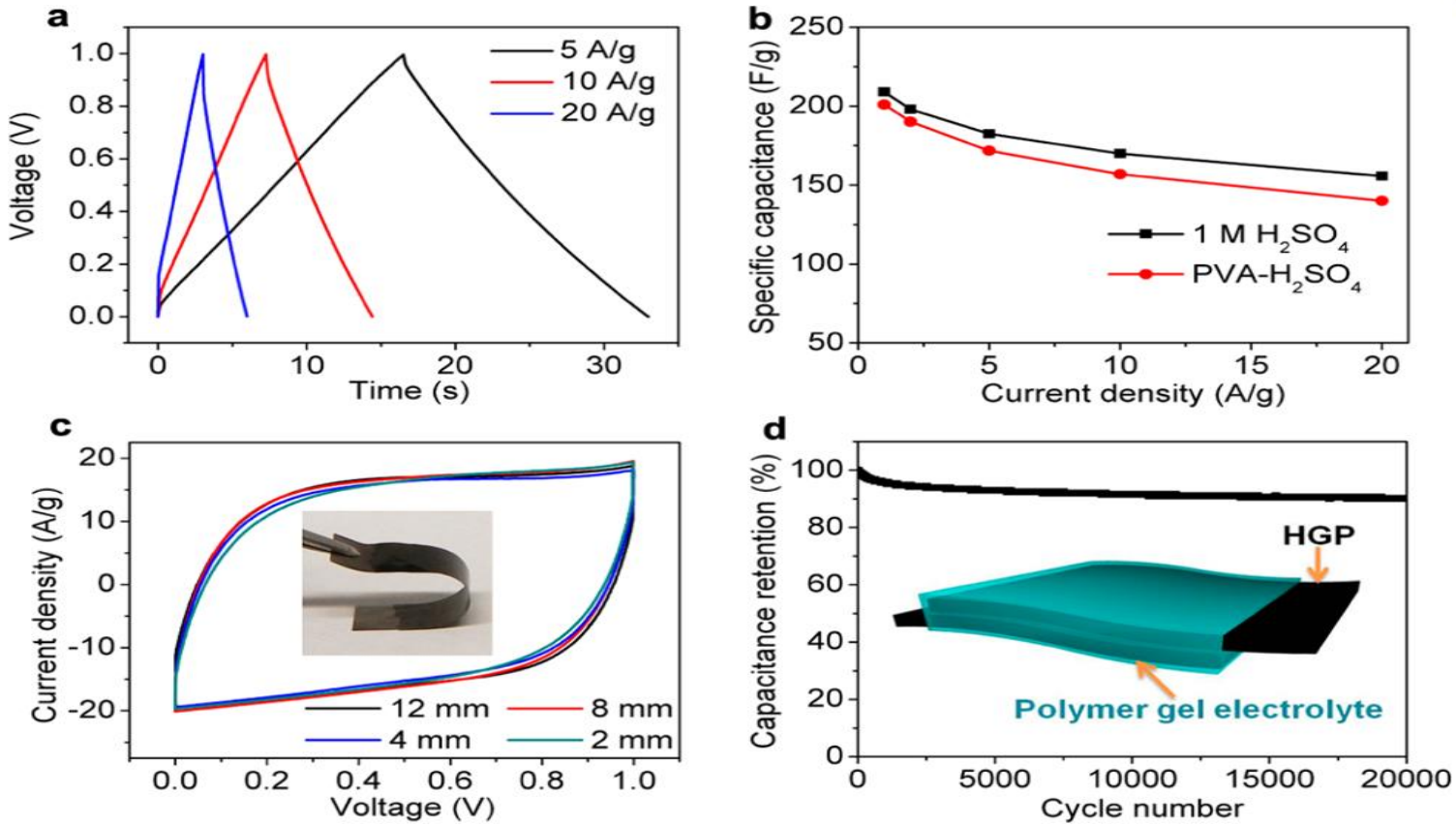

The entire flexible solid-state supercapacitor based on HGP showed a superior volumetric capacitance of 34 F/cm^3, which outperform most of previous reported results.

Nano Lett. 2015, 15, 4605.

Solution Processable Holey Graphene Oxide and Its Derived Macrostructures for High-Performance Supercapacitors

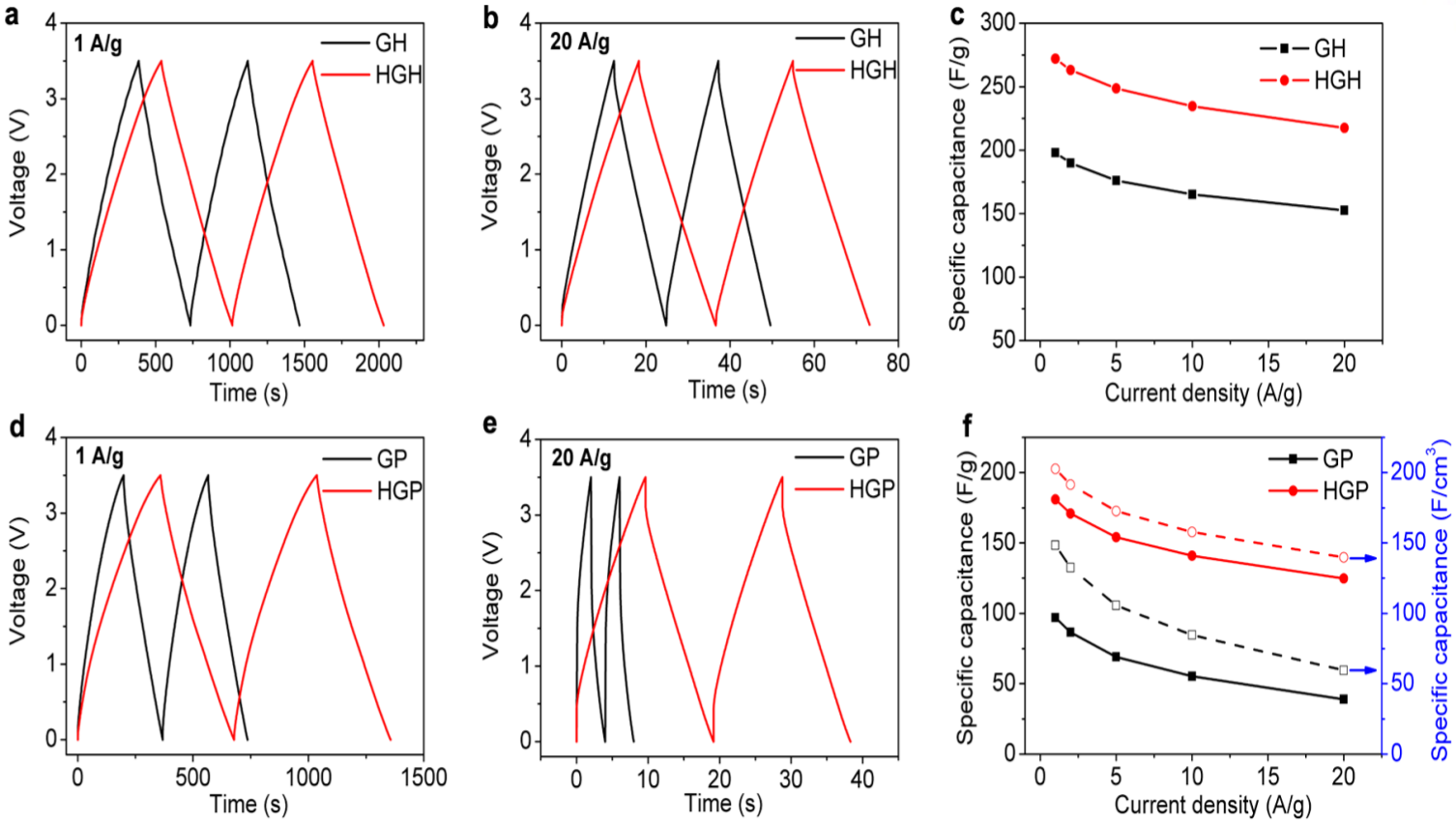

With $EMIMBF_4$/AN as organic electrolyte, a high energy density of 116 and 77 Wh/kg can be achieved for HGH and HGP, respectively. Moreover, the HGP could show a high volumetric capacitance of 203 F/cm^3 and a high volumetric energy density of 86 Wh/L.

Nano Lett. 2015, 15, 4605.

Three-Dimensional Graphene/Polyimide Composites

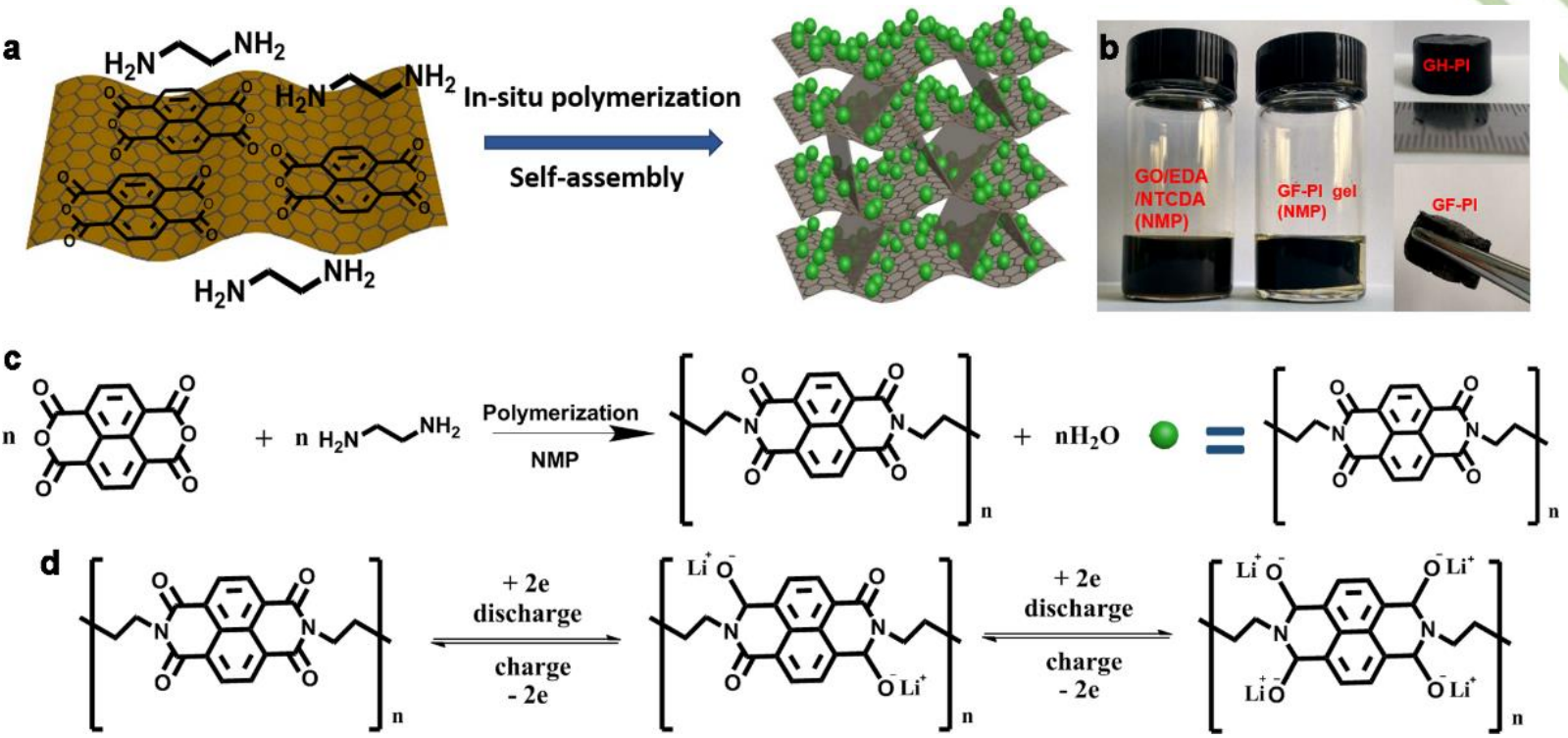

Schematic of the preparation process of GF-PI; (b) Photographs of precursor solution of GO, naphthalenetetracarboxylic dianhydride (NTCDA) and ethanediamine (EDA), the resultant GF-PI gel in N-Methyl-2-pyrrolidone (NMP) solution, the GH-PI with interior NMP exchanged by water, and the final GF-PI monolith after freeze-drying and annealing; (c) Synthetic route to PI; (d) Electrochemical redox mechanism of PI.

J. Mater. Chem. A, 2017,**5**, 2710-2716

Three-Dimensional Graphene/Polyimide Composites

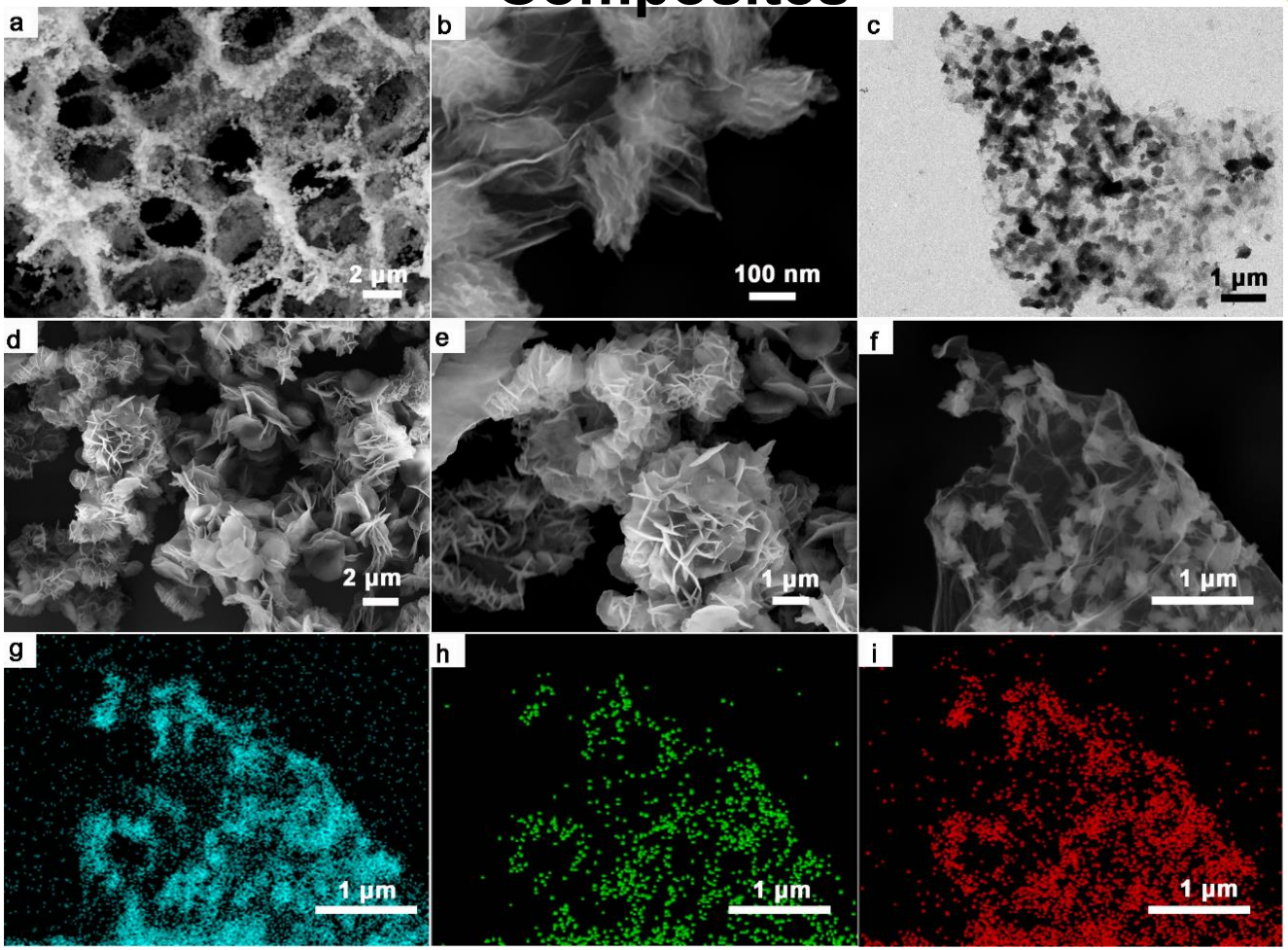

Low- and (b) high-magnification SEM images and (c) TEM image of GF-PI; (d) Low- and (e) high-magnification SEM images of pure PI; (f-i) Elemental mapping images of GF-PI (by SEM): Carbon (g), N (h), and O (i) distribution in the selected area.

J. Mater. Chem. A, 2017,**5**, 2710-2716

Three-Dimensional Graphene/Polyimide Composites

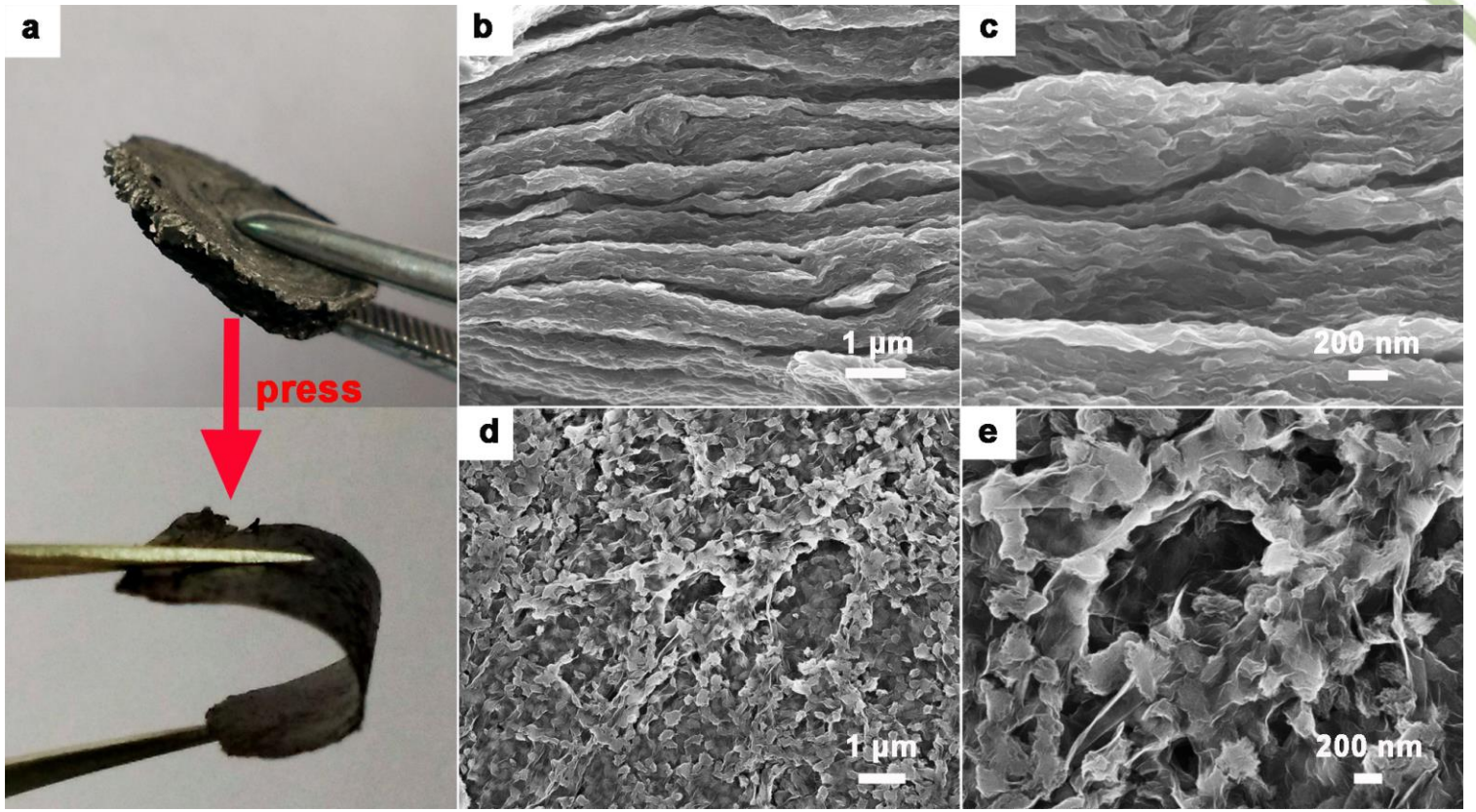

Preparation of a flexible binder-free GF-PI electrode. A piece of GF-PI (above) was mechanically pressed into a film electrode (down); SEM image of the side-view (b, c) and top-view (d, e) of the pressed GF-PI film.

J. Mater. Chem. A, 2017,**5**, 2710-2716

Three-Dimensional Graphene/Polyimide Composites

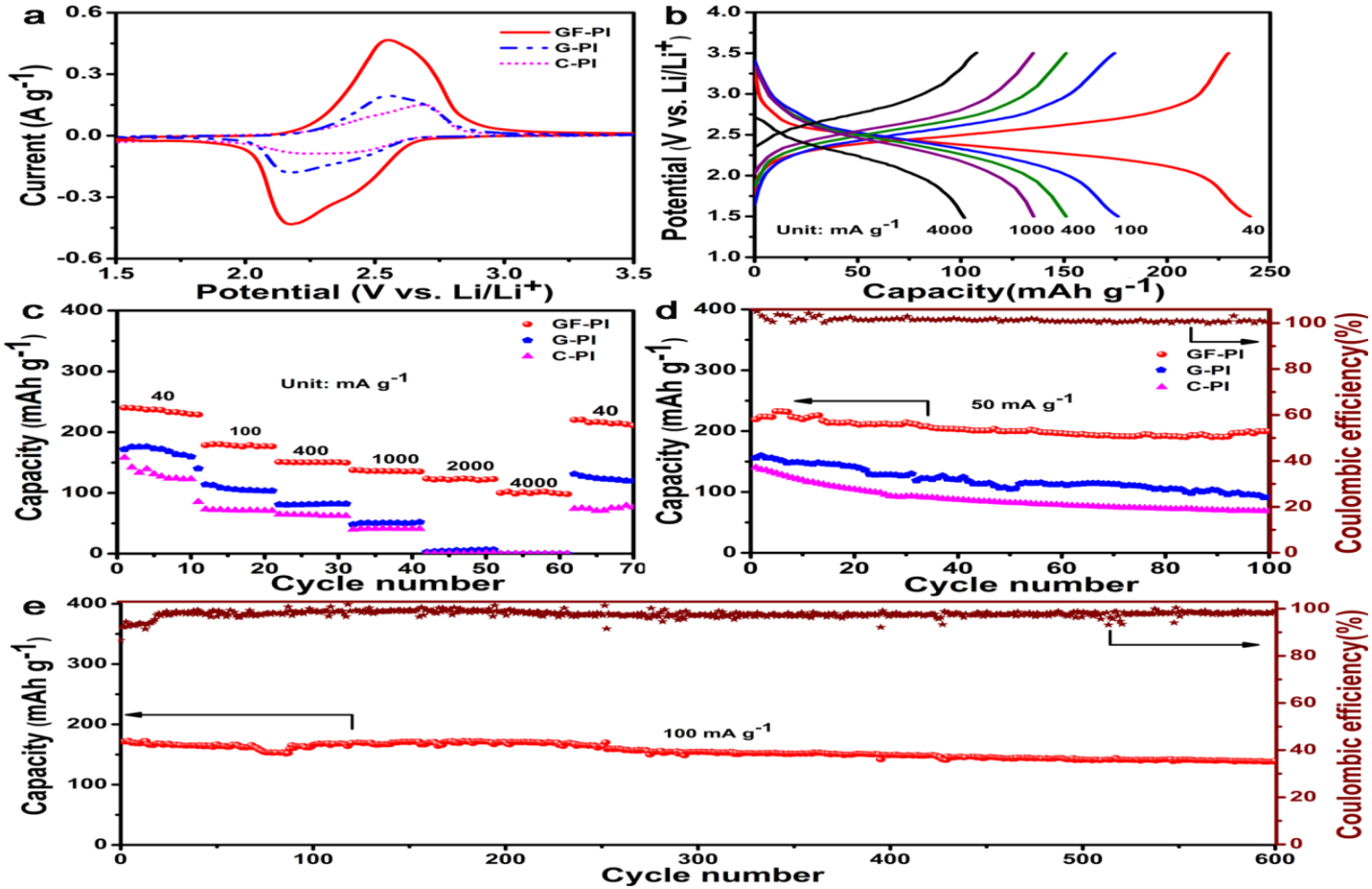

Electrochemical characterization of GF-PI as LIB cathode.

J. Mater. Chem. A, 2017,**5**, 2710-2716

Three-Dimensional Graphene/Polyimide Composites

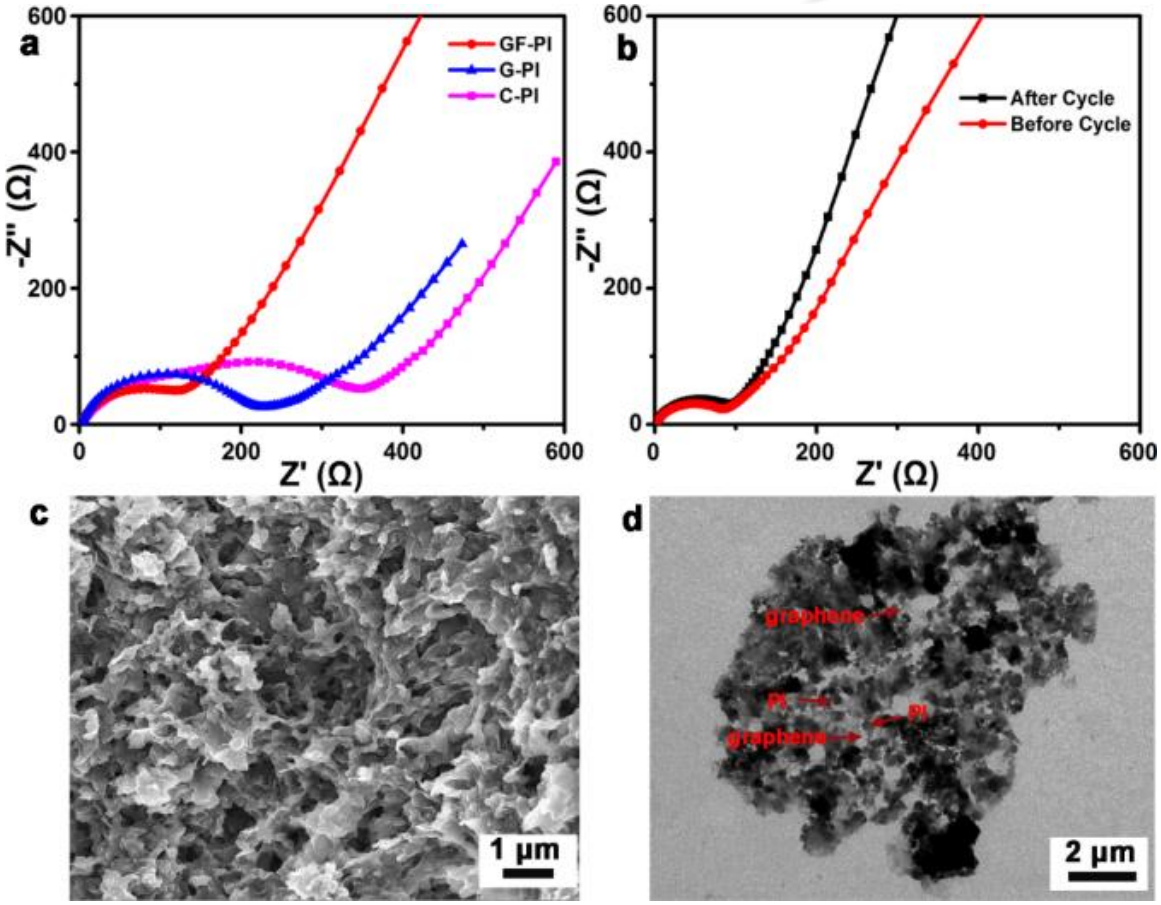

Nyquist plots for GF-PI, G-PI and C-PI electrodes; (b) Nyquist plots for GF-PI electrode before and after cycling test; (c) SEM and (d) TEM image of the GF-PI after 600 cycles.

J. Mater. Chem. A, 2017,**5**, 2710-2716

Three-Dimensional Graphene/Polyimide Composites

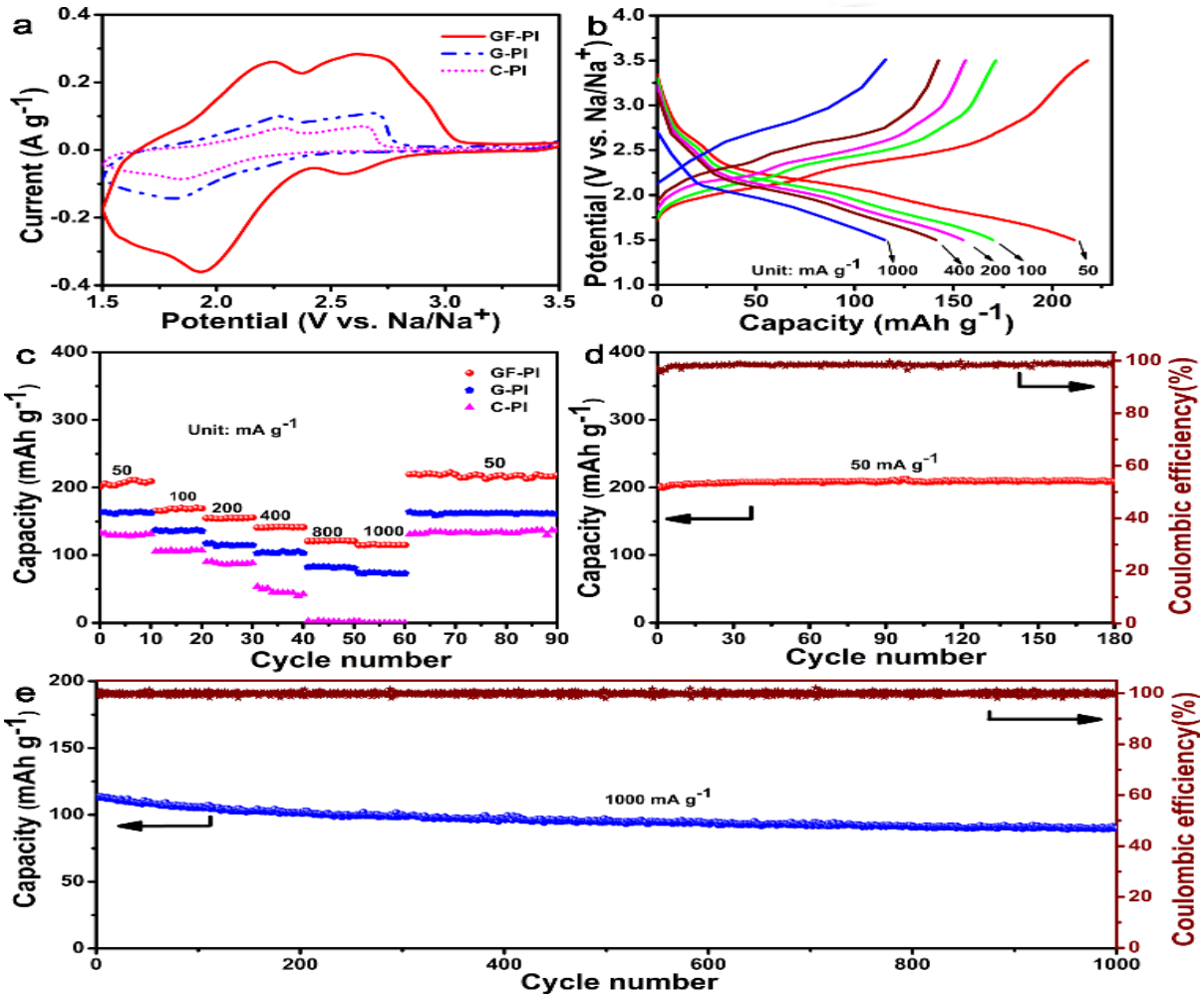

Electrochemical characterization of GF-PI as SIB cathode.

J. Mater. Chem. A, 2017,**5**, 2710-2716

Three-Dimensional Graphene/Poly (anthraquinonyl sulfide) (PAQS) Composites

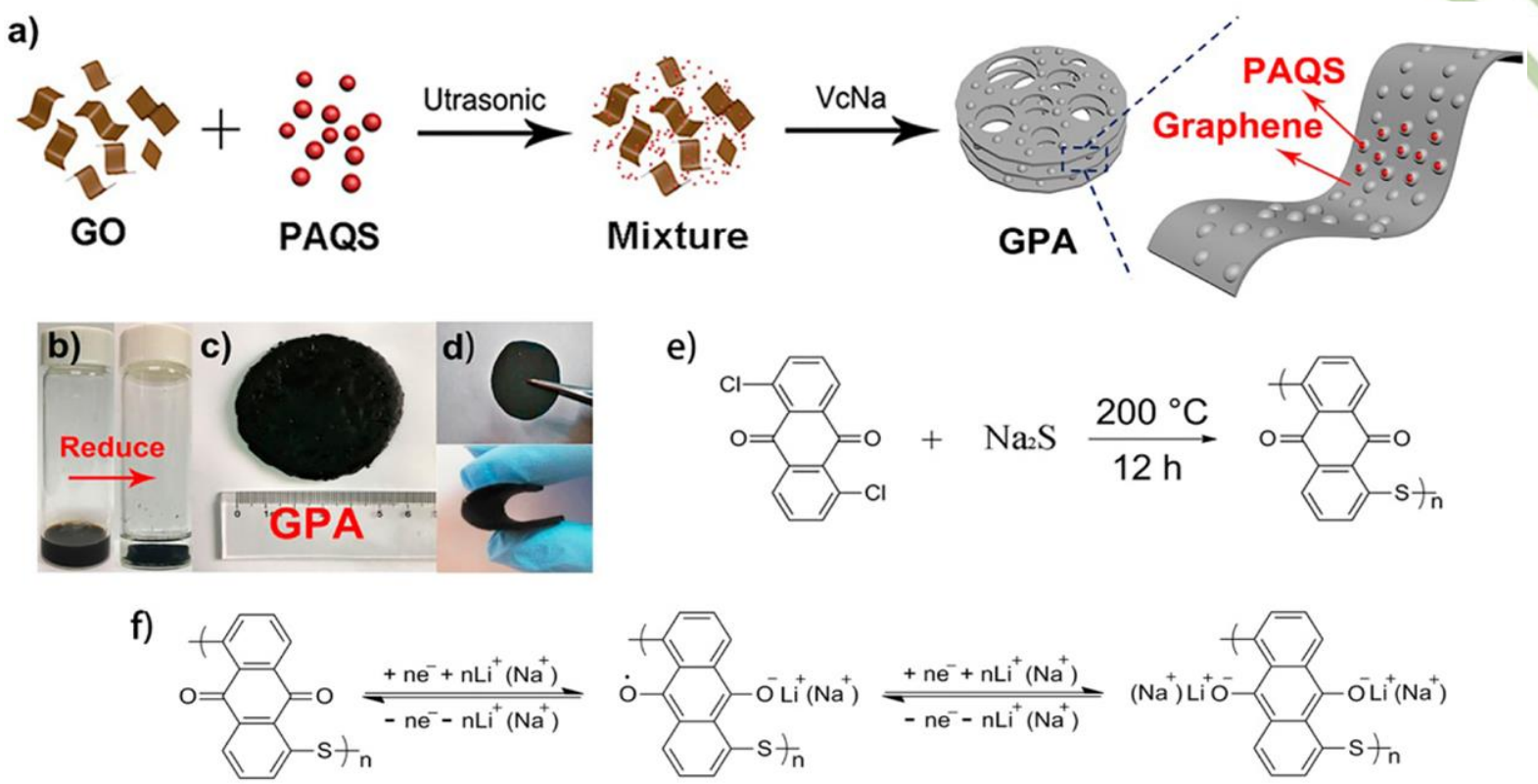

Schematic process of GPA. (b) Homogenous mixture of GO and poly (anthraquinonyl sulfide) PAQS in NMP and reduction and self-assembly of GO to form 3D graphene framework with encapsulated PAQS particles. (c) Freeze-dried aerogel of graphene/PAQS composite. (d) Preparation of a flexible binder-free GPA film electrode by mechanical pressing. (e) Synthetic route to PAQS. (f) Reversible redox mechanisms of PAQS in LIBs and SIBs.

ACS Appl. Mater. Interfaces 2017, 9, 15549−15556

Porous Fe_2O_3 Nanoframeworks Encapsulated within Three-Dimensional Graphene

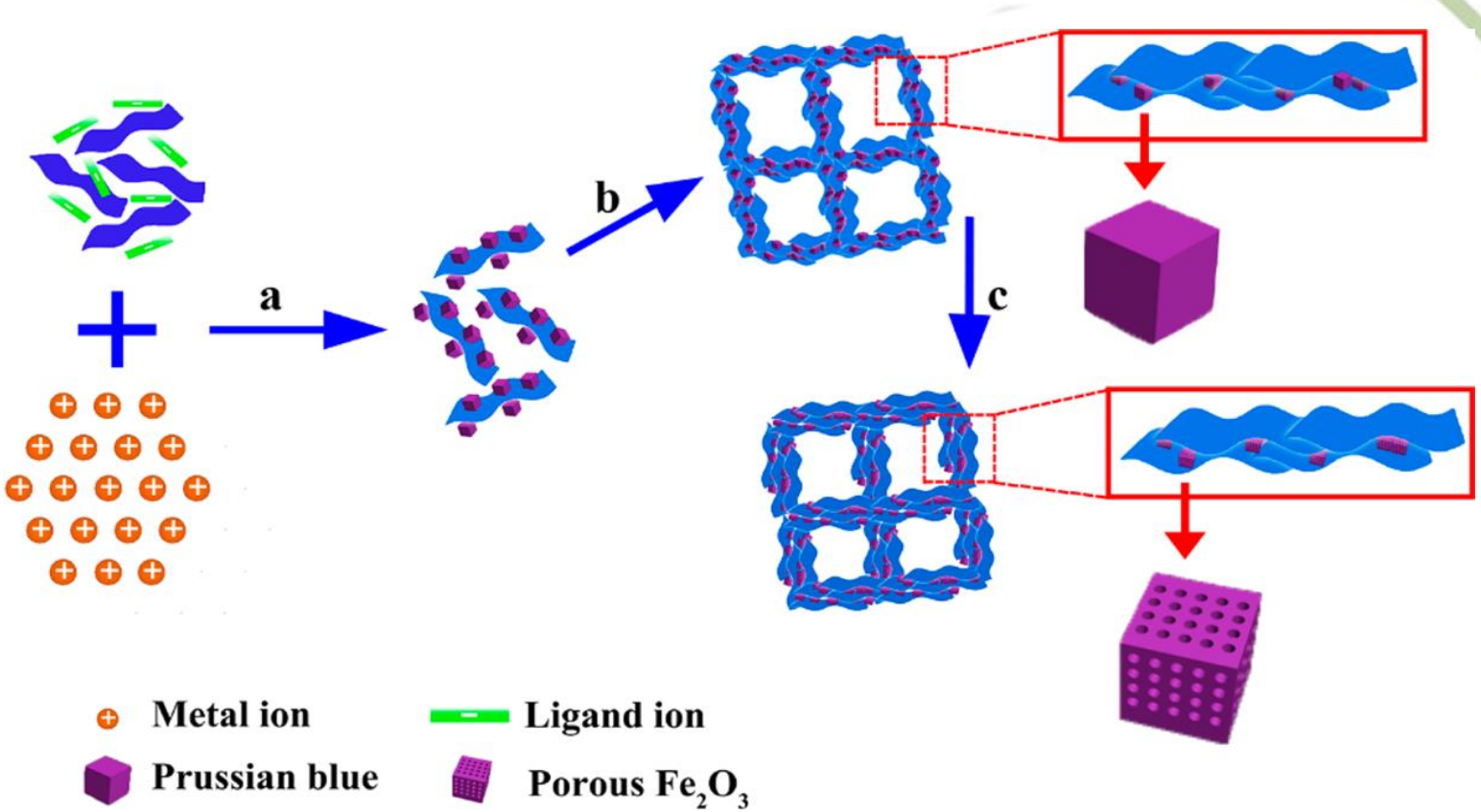

Schematic illustration of the preparation procedure of 3DG/Fe_2O_3. (a) Excessive metal ions induced combination, (b) self-assembly and spatially confined Ostwald ripening, and (c) thermal treatment under air condition.

ACS Nano: 2017, 11, 5140−5147

Porous Fe_2O_3 Nanoframeworks Encapsulated within Three-Dimensional Graphene

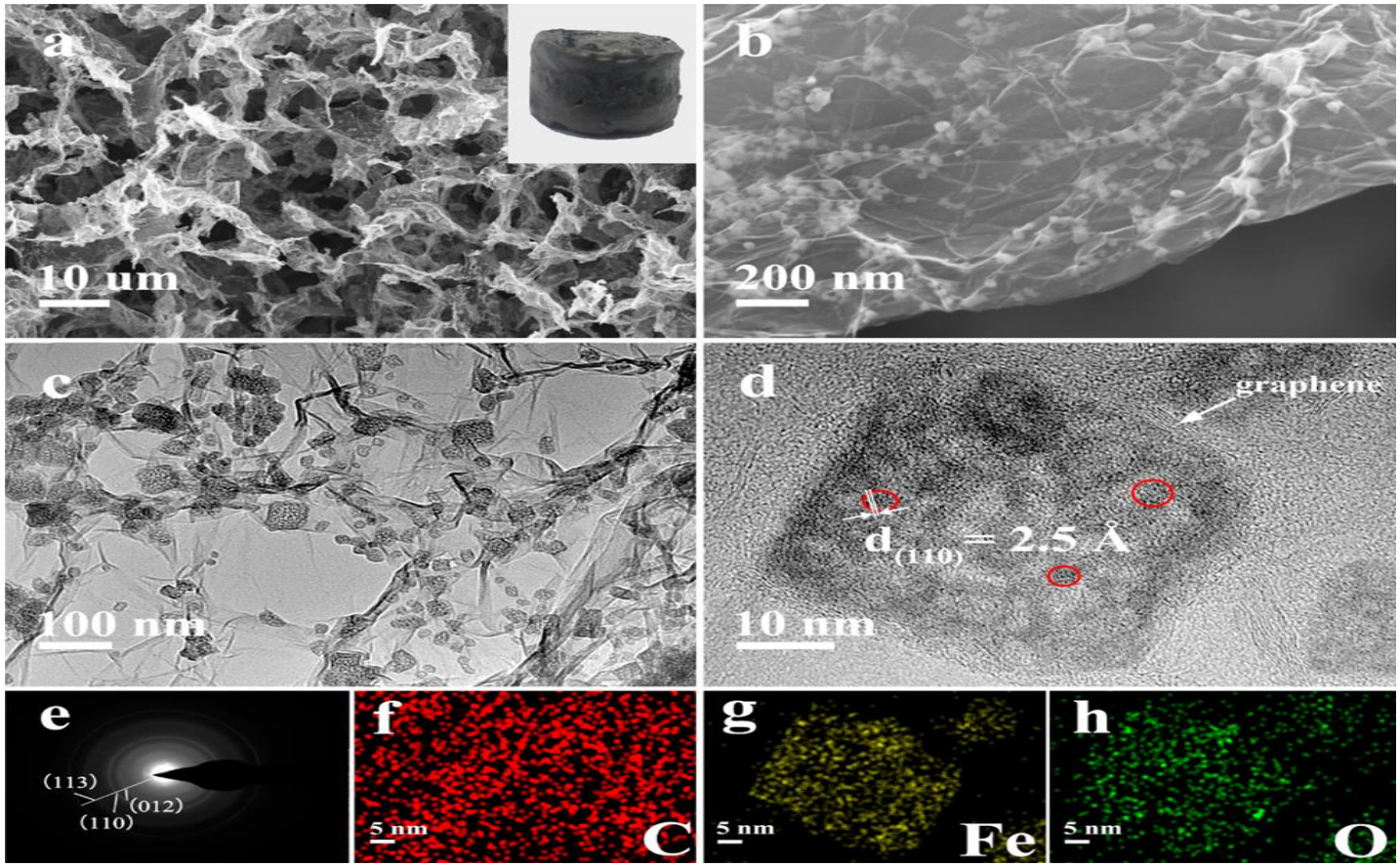

SEM and (c) TEM images of the microstructure of 3DG/Fe_2O_3 prepared by annealing of 3DG/PB at 250 °C for 2h. (d) HR-TEM image of 3DG/Fe_2O_3 and (e) the SAED pattern showing the poor crystallinity of Fe_2O_3. Elemental mapping images of C (f), Fe (g), and O (h) of 3DG/Fe_2O_3 composite shown in (d).

ACS Nano: 2017, 11, 5140−5147

Porous Fe_2O_3 Nanoframeworks Encapsulated within Three-Dimensional Graphene

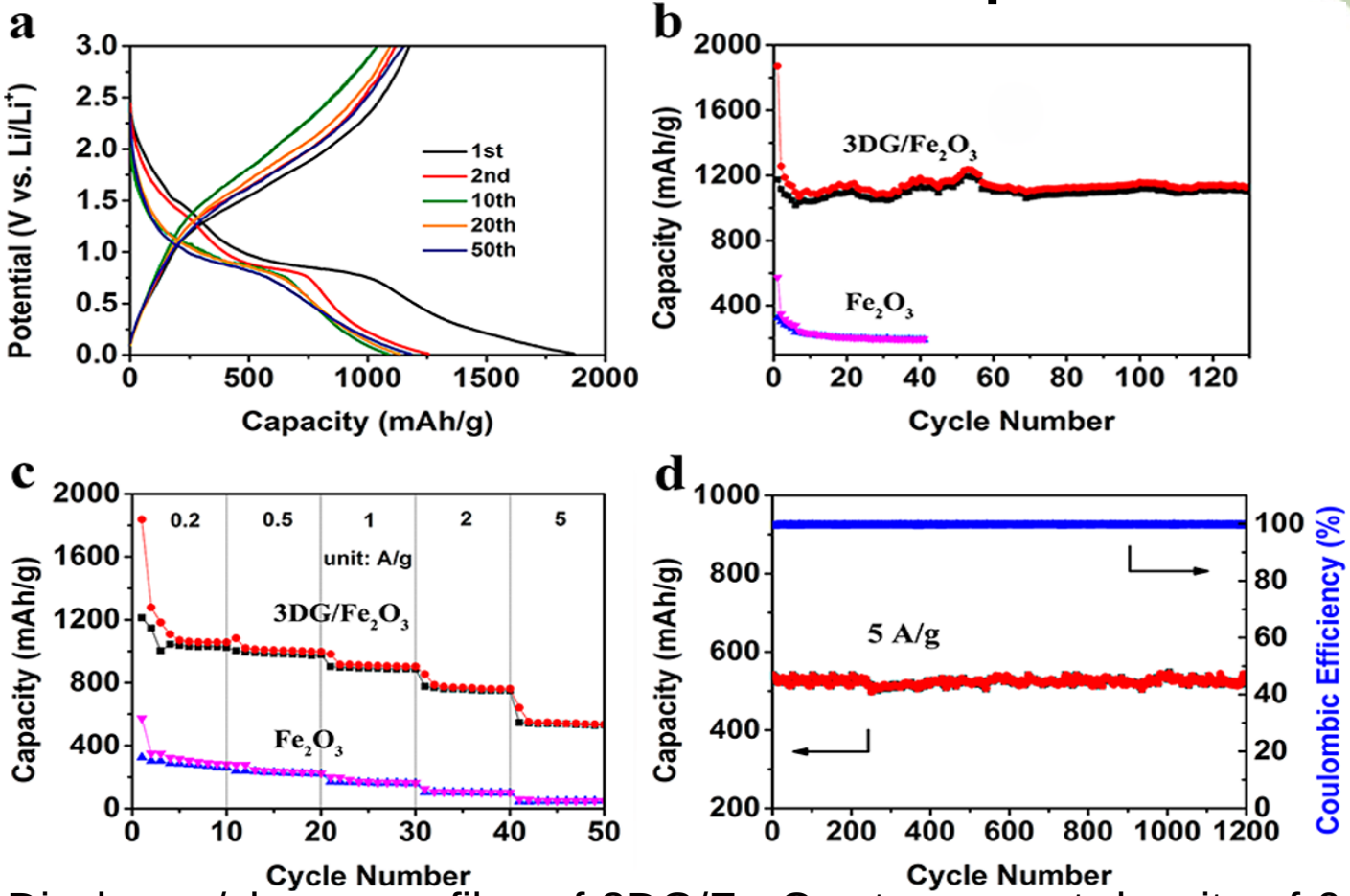

Discharge/charge profiles of $3DG/Fe_2O_3$ at a current density of 0.2 A/g. The cycling performance at 0.2 A/g (b) and rate performance (c) of $3DG/Fe_2O_3$ and Fe_2O_3, respectively. (d) Cycling performance of $3DG/Fe_2O_3$ at 5 A/g.

ACS Nano: 2017, 11, 5140−5147

Porous Fe_2O_3 Nanoframeworks Encapsulated within Three-Dimensional Graphene

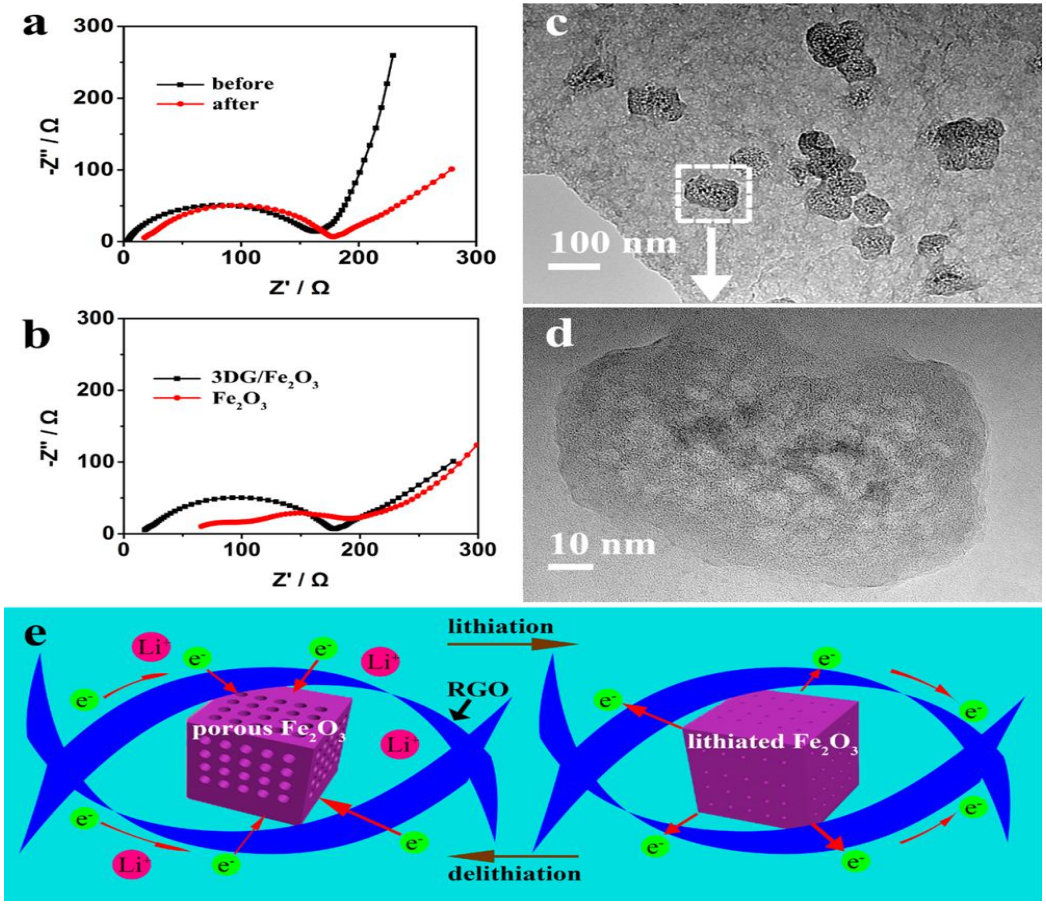

The Nyquist plots of 3DG/Fe_2O_3 before and after cycling test. (b) The Nyquist plots of 3DG/Fe_2O_3 and Fe_2O_3 after cycling test. (c) TEM image of 3DG/Fe_2O_3 and (d) higher magnification image of a single Fe_2O_3 nanoframework under delithiation state after cycling test. (e) The schematic of delithiation/lithiation reactions of 3DG/Fe2O3

ACS Nano: 2017, 11, 5140−5147

Three-Dimensional Holey-Graphene/Niobia Composite Architectures

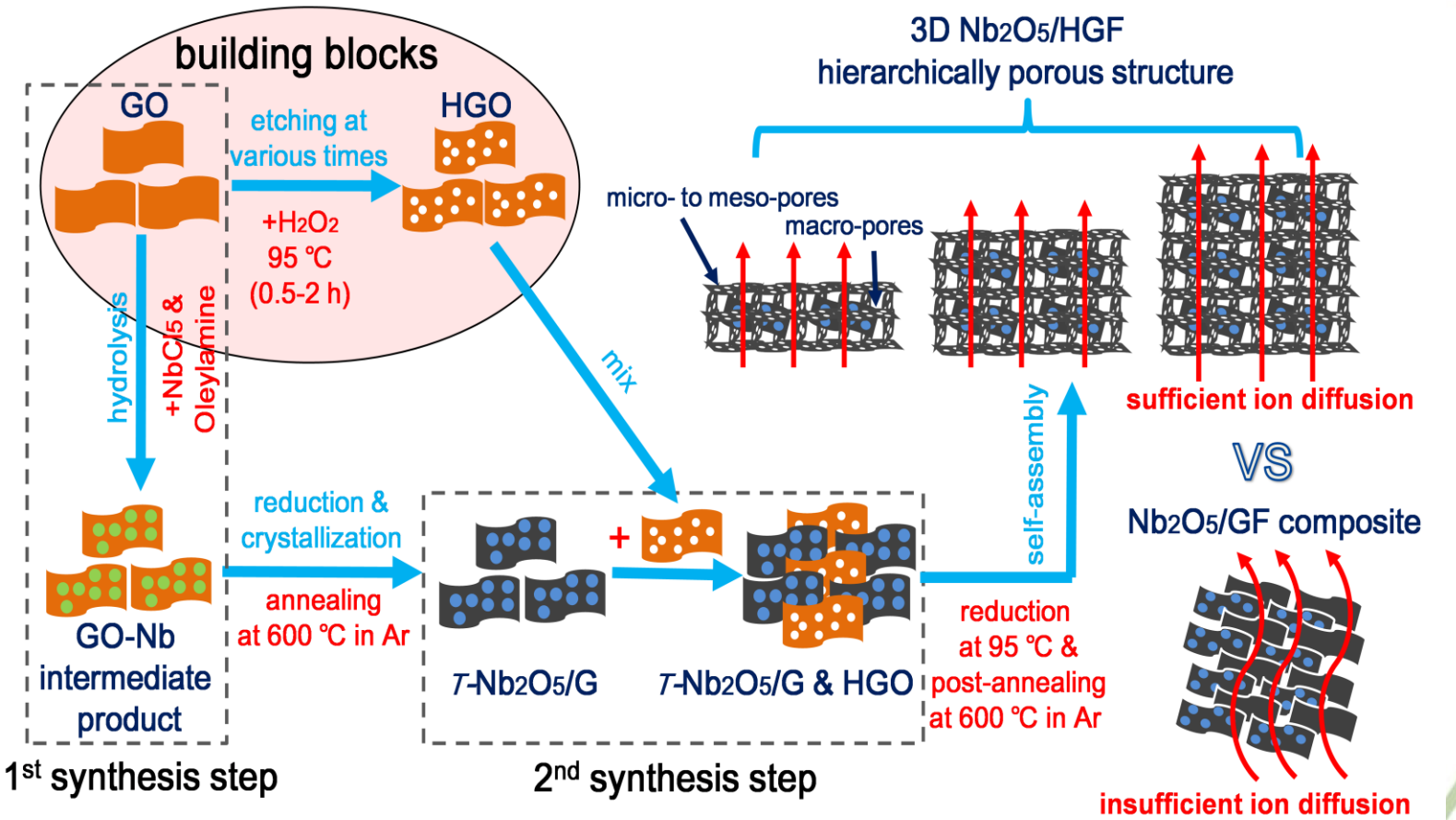

Science 356, 599–604 (2017)

Three-Dimensional Holey-Graphene/Niobia Composite Architectures

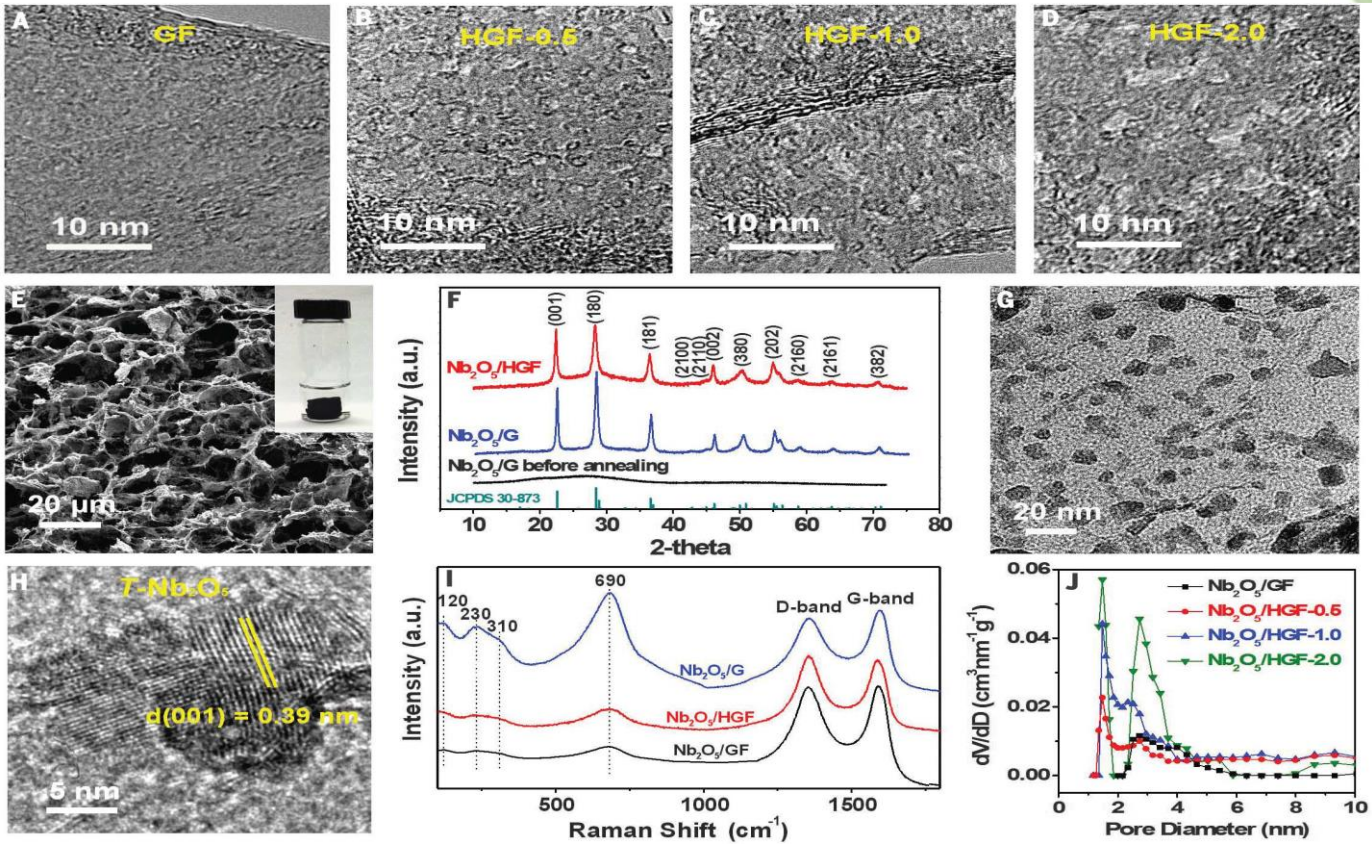

TEM images of graphene sheets with tailored pores obtained by etching in H_2O_2 for 0, 0.5, 1.0, and 2.0 hours, respectively, (E) Cross-sectional image of Nb_2O_5/HGF composite shows 3D hierarchically porous structure, (F) XRD patterns, (G) TEM image of graphene sheets with uniformly decorated T-Nb_2O_5 nanoparticles, (H) HR-TEM image of T-Nb_2O_5 nanoparticles, (I) Raman spectra of Nb_2O_5/G powder after thermal annealing, and freestanding Nb_2O_5/GF and Nb_2O_5/HGF electrodes. The D and G bands are characteristic of RGO; The Raman bands at 120, 230, 310, and 690 cm−1 further confirm the orthorhombic phase of T-Nb_2O_5. (J) Comparison of DFT pore size distributions. The prominent pore size shifts from micropores (~1.5 nm) to mesopores (2.7 nm) for the composite prepared from HGO with increasing etching time.

Science 356, 599–604 (2017)

Three-Dimensional Holey-Graphene/Niobia Composite Architectures

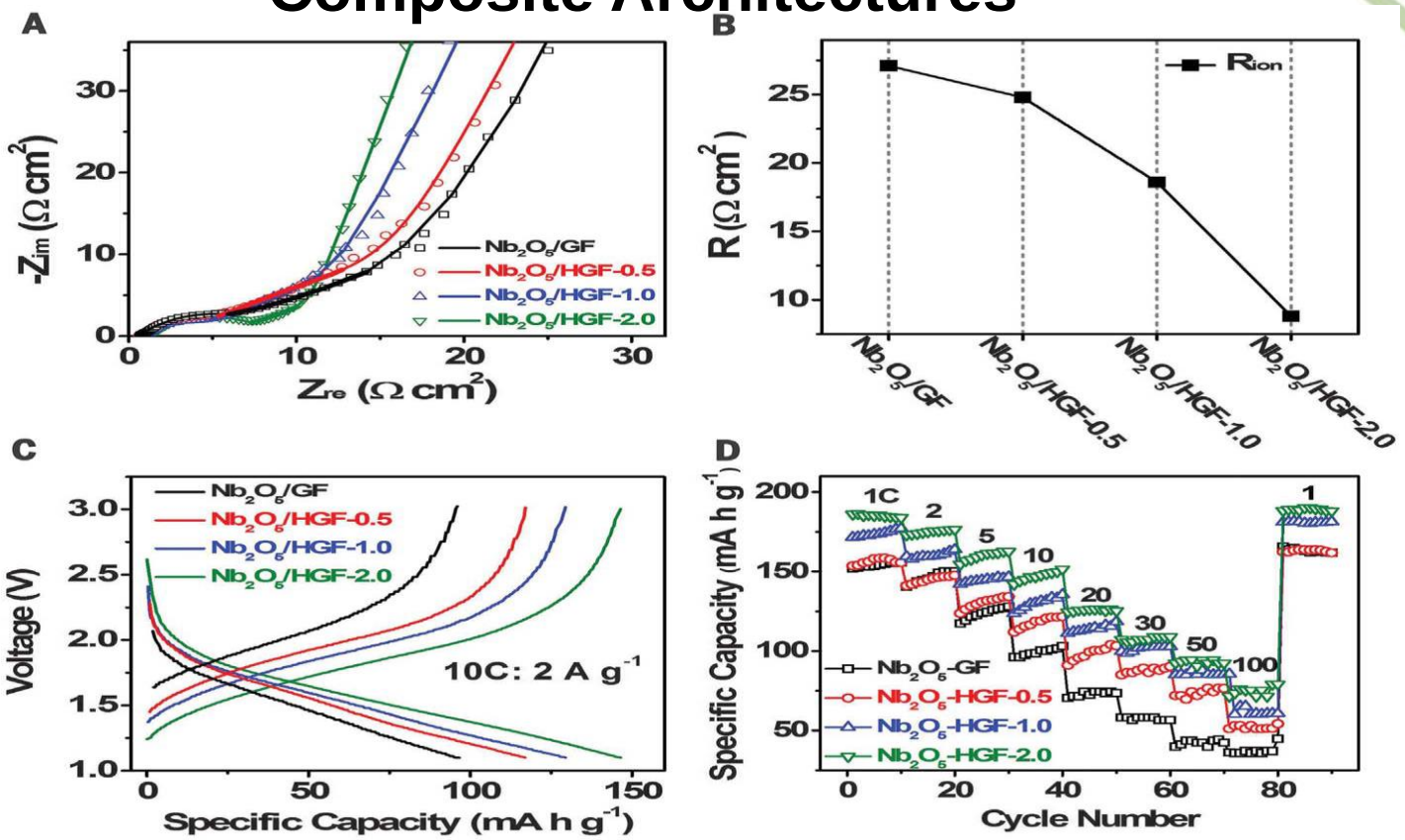

Comparison of Nyquist plots obtained from potentiostatic EIS of a symmetric cell using two identical electrodes (11 mg cm^{-2}) at a SOC 0%. The projection of the 45° slope in the high-frequency region is used to determine the ionic resistance for the electrolyte-filled porous architectures in a nonfaradaic process.The open symbols and solid lines represent the experimental and simulation results, respectively. (B) The ionic resistance (Rion) as a function of the porosity of the electrode materials. With increasing porosity, the ionic resistance is reduced substantially. (C) Galvanostatic charge-discharge curves of electrodes with tunable nanoporosity at a rate of 10C in the voltage window 1.1 to 3.0 V (versus Li/Li+). (D) Comparison of specific capacities (normalized by the total mass of the electrodes) at various rates (1 to 100C) for composite electrodes with tunable nanoporosity.

Science 356, 599–604 (2017)

Three-Dimensional Holey-Graphene/Niobia Composite Architectures

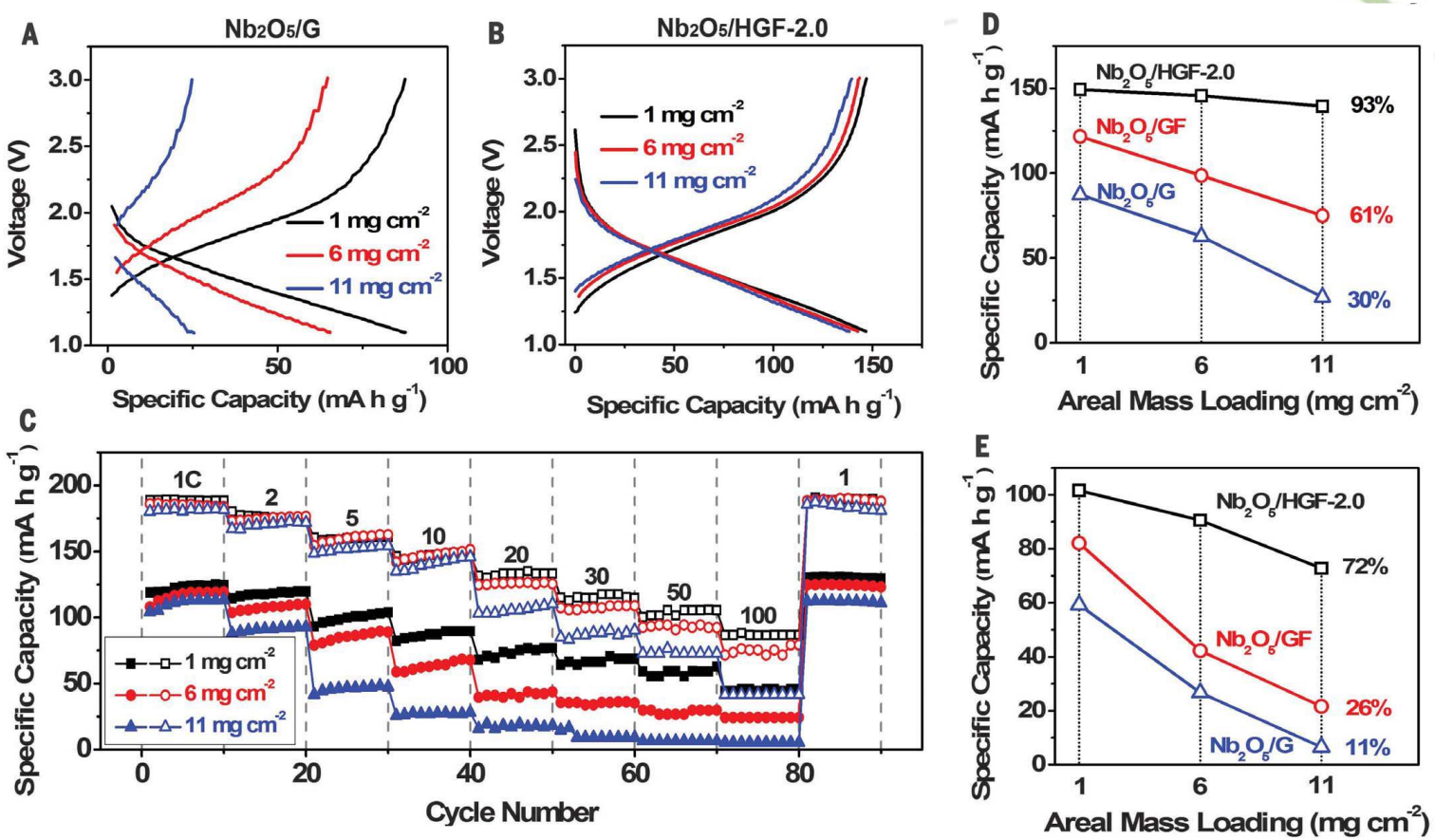

Effects of mass loading on electrochemical characteristics. (A and B) Galvanostaticcharge-discharge curves for (A) the Nb2O5/G control electrode and (B) the Nb2O5/HGF-2.0 electrode at a rate of 10C for the mass loadings of 1, 6, and 11 mg cm−2. (C) Comparison of the rate performance between 1C and 100C for Nb2O5/HGF-2.0 (open) and Nb2O5/G (solid) electrodes under different mass loadings (1, 6, and 11 mg cm−2). (D and E) Retention of specific capacity at (D) 10C and (E) 50C as a function of mass loading for three different electrodes. The properties of Nb2O5/HGF-2.0 and Nb2O5/GF electrodes were normalized by the total mass of the electrode materials (free of conductive additives and binders); the control Nb2O5/G electrodes were normalized by the total mass of the electrode materials (including binders and conductive additives).

Science 356, 599–604 (2017)

Conclusions

- The first direction is to integrate active/synergetic nanomaterials

- The second direction is to improve the overall electrical conductivity of metal oxide films/arrays to the largest extent by integrating with diverse conducting agents

- The third direction is the innovation in electrode structure design. For some future applications, good electrodes are expected to be lightweight, full of porosity, mechanically flexible but still robust enough to maintain the power supply.

Thank you for your attention!